Tampere University

Iida Mäki-Karvia

IMPEDANCE PNEUMOGRAPHY IN RESPIRATION MONITORING

Bachelor's Thesis
Faculty of Medicine and Health Technology
Antti Vehkaoja
05/2022

ABSTRACT

Iida Mäki-Karvia: Impedance pneumography in respiration monitoring
Bachelor's Thesis
Tampere University
Biotechnology and biomedical engineering
May 2022

Respiration monitoring provides health care professionals essential information about patients' condition and can help diagnosing pulmonary diseases. The most reliable methods for assessment are obtrusive and include masks and can require performing manoeuvres that limit the usability with uncooperative patients like children or unconscious. In contrast, in hospital wards respiration rate and effort are intermittently assessed only visually during rounds at patient rooms leading to poor frequency of recording. Hence, early signs of deterioration in condition are often missed.

Bioimpedance have been studied as a continuous and unobtrusive method for respiration monitoring. The technique is based on differences in electrical properties of tissues. A small current is fed through the body and voltage across is measured. Respiration and cardiac functions affect current flow and thus change the total impedance. Frequency of the applied current and geometry of the thorax cause also variation in the signal. When using bioimpedance to assess respiratory functions the method is called impedance pneumography. Despite of being an established and widely used method, there is ongoing research to improve its performance. One major challenge is its susceptibility to movement. However, signal processing algorithms advance all the time making development of wearable applications also possible.

In this study, respiration is measured with bioimpedance and compared to signal from pneumotachometer. Two different electrode configurations were used to evaluate their performance in different positions, in supine, sitting and walking stationary. The study protocol included alternation between thoracic and diaphragmatic breathing at different depths. Respiration rates were determined with peak detection, advanced counting and Fast Fourier Transform (FFT) algorithms and their performances were compared.

The results show that respiration rates were most accurately measured during supine position with Mason-Likar arm electrodes. No significant differences between thoracic and diaphragmatic breathing were seen whereas shallow breathing was occasionally hard to detect. The peak detection algorithm performed best having mean absolute error (MAE) of 0.47, 1.12 and 1.23 breaths per minute (bpm) for lying, sitting and walking, respectively. However, MAE values of FFT method were not comparable to other methods in most of the cases.

Comparison between electrode configurations is not straightforward, as the measurements were not made simultaneously. Also, the study involved only relatively young and healthy subjects which are not the most abundant age group needing monitoring at hospitals. When considering patient monitoring applications, future studies should involve subjects with wider range of characteristics to obtain more definitive results about the performance of the impedance pneumography.

Keywords: Impedance pneumography, Respiration monitoring, Respiration rate, Electrode configuration

TIIVISTELMÄ

Iida Mäki-Karvia: Impedance pneumography in respiration monitoring
Kandidaatintyö
Tampereen yliopisto
Bioteknologian ja biolääketieteen tekniikan tutkinto-ohjelma
Toukokuu 2022

Hengitystä monitoroimalla saadaan tärkeää informaatiota potilaan terveydentilasta sekä apua keuhkosairauksien diagnosointiin. Tällä hetkellä luotettavimmat menetelmät häiritsevät luonnollista hengitystä ja saattavat vaatia erityisiä hengityskuvioita, jotka eivät onnistu yhteistyökyvyttömiltä potilailta kuten lapsilta tai vakavasti sairailta. Toisaalta sairaaloiden osastoilla hengitystaajuutta ja hengityksen vaikeutta saatetaan ajoittain arvioida ainoastaan visuaalisesti tarkastuskierrosten aikana, jolloin tuloksien väli saattaa venyä pitkäksi eikä muutoksia huomata ajoissa.

Bioimpedanssimenetelmä tarjoaa keinon jatkuvaan hengityksen monitorointiin häiritsemättä sitä. Tekniikka perustuu kudosten erilaiseen kykyyn vastustaa sähkövirran kulkua, ja sen avulla voidaan saada monesta kehontoiminnosta tietoa. Hengityksen analysoinnissa menetelmästä käytetään nimitystä impedanssipneumografia. Käytännössä kehoon syötetään pieniamplitudista virtaa ja mitataan jännitettä mittapisteiden välillä. Hengityksen aiheuttamat muutokset vaikuttavat sähkövirran kulkuun ja näin ollen muuttavat impedanssisignaalia. Myös syötetyn virran taajuus sekä rintakehän muoto vaikuttavat havaittuun impedanssiin. Vaikka menetelmä on jo vakiintunut ja laajalti käytössä, tutkijat pyrkivät jatkuvasti parantamaan bioimpedanssin mittaustekniikkaa. Yksi menetelmän heikkouksista on sen alttius liikkeestä aiheutuville häiriöille. Signaalinkäsittelymenetelmät kehittyvät kuitenkin jatkuvasti mahdollistaen myös tutkimuksen bioimpedanssin käytöstä puettavissa laitteissa.

Tässä tutkimuksessa mitattiin hengitystä bioimpedanssin avulla ja verrattiin saatua signaalia pneumotakometrillä kerättyyn referenssiin. Mittauksissa käytettiin kahta eri elektrodien sijoittelua ja arvioitiin niiden toimivuutta eri asennoissa: selinmakuulta, istualtaan sekä paikallaan kävellessä. Mittausten aikana tutkittavat hengittivät eri syvyyksillä ja vaihtelivat pallea- ja rintahengityksen välillä. Saadusta datasta arvioitiin hengitystaajuutta peak detection, advanced counting ja Fast Fourier Transform -algoritmeilla ja vertailtiin niiden toimivuutta.

Tutkimuksessa havaittiin, että luotettavin arvio hengitystaajuudesta saatiin makuuasennossa Mason-Likar käsielektrodeilta mitattaessa. Pallea- ja rintahengityksen välillä ei havaittu merkittäviä eroja, kun taas pinnallista hengitystä oli ajoittain vaikea havaita impedanssisignaalista. Peak detection -algoritmin suoriutui parhaiten käytetyistä metodeista. Tällä menetelmällä keskimääräinen absoluuttinen virhe oli 0.47 hengitystä minuutissa (bpm) makuulta, 1.12 bpm istualtaan ja 1.23 bpm kävellessä. FFT-algoritmilla ei saatu vertailukelpoisia arvoja hengitystiheydestä johtuen todennäköisesti liian suuresta ikkunan pituudesta.

Elektrodipaikkojen vaikutusta on hankala arvioida suoraviivaisesti, sillä mittauksia ei tehty samanaikaisesti. Tutkimuksessa oli mukana ainoastaan suhteellisen nuoria ja hyväkuntoisia henkilöitä. Tällaisilta tutkittavilta mahdollisesti saadaan parempia tuloksia kuin ikääntyneiltä tai ylipainoisilta. Potilasmonitorisovelluksia ajatellen seuraaviin tutkimuksiin kannattaisi ottaa mukaan ominaisuuksiltaan laajempi joukko tutkittavia, jotta saataisiin kattavampi näyttö impedanssipneumografian suorituskyvystä.

Avainsanat: Impedanssipneumografia, Hengityksen monitorointi, Hengitystiheys, Elektrodikonfiguraatio

CONTENTS

LIST OF FIGURES

1. INTRODUCTION

Respiration is one of the basic vital signs. It is essential part of a system maintaining the homeostasis within the body while providing oxygen for the tissues and excreting carbon dioxide. Nonetheless, respiration monitoring is frequently overlooked in hospitals even though a shift in patients' condition cause more significant changes in respiration rate (RR) than in heart rate or blood pressure. For example, high respiratory rate has been found to precede severe illnesses such as cardiac arrest or other symptoms needing intensive care. (Cretikos et al. 2008) This implicates that constant monitoring of RR could provide critical information about how patients' condition is proceeding. In best case scenario, the worsening of the condition could be avoided when medical reviews can be performed earlier, thus lives and resources would be saved.

There are various methods for respiration rate detection. These methods are based on for example pressure, temperature change, air flow or chest and abdominal movement or RR can be derived from other signals like electrocardiogram (ECG). Yet these methods have their drawbacks and often employ nasal cannulas or masks limiting the use in long-term monitoring. (AL-Khalidi et al. 2011) When measuring flow and respiration pattern related parameters spirometry is deemed as the golden standard. However, this method partially blocks the airway thus affects the respiration pattern. To get valid results with spirometry, the patient needs to perform specific breathing manoeuvres. This restricts the usability with uncooperative patients like children and unconscious or seriously ill patients. (Jeyhani, Vuorinen, Noponen et al. 2016) Thus, alternative methods have been studied.

One promising option is impedance pneumography (IP), where lung functions are assessed by measuring impedance changes due respiration. This non-invasive method does not require altering the normal breathing but is used during tidal breathing. IP has low costs and permit portable monitoring (Khalil et al. 2014). Hence, long-term measurements can be done which enable more extensive assessment of lung functions to help diagnosing. However, bioimpedance measurement is not faultless either. IP is especially

prone to motion artefacts which bring also challenges to continuous monitoring. Respiration with slow frequency or low amplitude can be readily left undetected with IP which is problematic especially in applications directed to hospital use as anaesthesia and opioid based pain medication depress the ventilation. (Seppä 2014) When considering flow and volume measurements, IP requires individual calibration before use if absolute values are to be obtained. (Berkebile et al. 2021) Nonetheless, IP appears promising method for respiration monitoring and solutions to its weaknesses are researched.

The objective of this study was to evaluate the effect of a subject posture and electrode placement to impedance signal and compare the performance of few processing algorithms on RR detection. RR was measured in supine and sitting positions and during walking. Two different electrode configurations were used, and respiration was measured during diaphragmatic and thoracic breathing. The data acquisition was done with Biopac device (EBI100C), and a pneumotachometer is used to gather a reference signal. Consistency of the IP signal with reference is examined, and validity of the RR detection algorithm is assessed.

First, in Chapter 2 the theory and relevance of bioimpedance measurements are presented. In addition, prior studies with different setups are described. The 3rd chapter describes the experimental setup and methods used in this study. In Chapter 4, the obtained results are presented and observations about them are made. Chapter 5 concludes the thesis work.

2. THEORETICAL BACKGROUND

2.1 Fundamentals of bioimpedance

Impedance is a basic electrical variable which describes the ability of a circuit to resist current flows. According to Ohm's law

$$Z = \frac{U}{I} \ , \tag{1}$$

where *Z* is impedance, *U* is voltage and *I* current, impedance is directly proportional to voltage. This same law applies in human body; if a current is fed through the body and the voltage across it is measured, a value for impedance is calculated as their ratio. (Seppä 2014, p. 9)

The impedance seen in Equation 1 consists of two parts: resistance and reactance. As resistance tells how currents are opposed, reactance describes reactivity to current changes. Hence, impedance is defined as followed

$$Z = R + iX, \tag{2}$$

where *R* is resistance and *X* reactance of a component. Furthermore, reactance is determined as

$$X = X_C - X_L = \frac{1}{\omega C} - \omega L, \tag{3}$$

where X_C is reactance of a capacitor, X_L reactance of an inductor, ω angular frequency, *C* is capacitance and *L* inductance. (Mansfield 2011, Chapter 17) From Equation 2 can be seen that impedance is an imaginary quantity. Total magnitude of the impedance is defined as an absolute value of *Z* as in Equation 4 and the phase angle can be calculated from basic trigonometric functions according to Equation 5.

$$|Z| = \sqrt{R^2 + X^2} \tag{4}$$

$$\phi = \arctan\left(\frac{X}{R}\right) \tag{5}$$

Also, what is notable is that the impedance of a resistor is constant but with capacitor and inductor frequency dependent. (Mansfield 2011, Ch. 17)

Tissues are generally electrically modelled as a parallel connection of a resistor and a complex of resistor and a capacitor connected in series (Brown et al. 1994). The equivalent circuit for the model is illustrated in Figure 1.

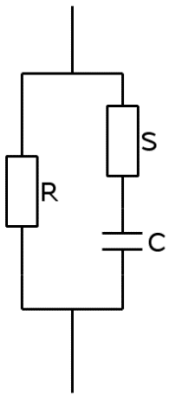

Figure 1. *Equivalent circuit modelling electrical properties of tissue. Reproduced from Brown et al. 1994.*

In Figure 1 the resistor *R* represents the resistance of extracellular matrix, *S* the resistance of intracellular path and *C* the capacitive properties of cell membranes (Brown et al. 1994). As earlier illustrated in Equation 3, the capacitor in the model causes the impedance of the body to be frequency dependent.

The frequency of the alternating current sent to the body determines the behaviour of the current within the tissues. Impedance of a capacitor approaches infinity when the frequency decreases. This means that a low-frequency current will not pass the cell membranes but flows between the cells in the extracellular matrix. As the frequency increases capacitive properties of the cell membrane lets current flow into the cells. These different paths for current flow are illustrated in Figure 2. (Grimnes & Martinsen 2015, Chapter 4)

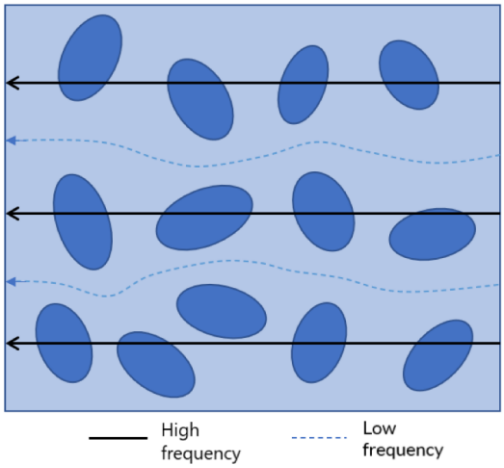

Figure 2. *Current paths in the tissues. Reproduced from Grimnes & Martinsen, 2015.*

Impedance is also affected by the geometry and resistivity of the specimen. Resistance of a conductive material can be calculated from following equation

$$R = \rho \frac{l}{A}, \tag{6}$$

where ρ is resistivity of the material, l length and A the cross-sectional area. As human body is not a homogenous conductor but consists of different tissues, the resistivity is not constant between the measuring points. (Grimnes & Martinsen 2015, Chapter 4) Yet a linear relationship between lung volume and resistivity can be approximated (Nopp et al. 1997) enabling the use of bioimpedance measurements with respiration monitoring. The effect of cross-sectional area must be considered when deciding an electrode configuration as the geometry of the chest brings intersubjective variation to the signal. (Grimnes & Martinsen 2015, Chapter 4). Also, differences in thorax geometry between genders cause inconsistencies with IP signal (Mlynczak & Cybulski 2017).

Biological matters can have highly organized structures which can be seen for example in muscles, nerves and blood vessels. This kind of orientation influence the electric properties of the tissue such as the conductivity. Consequently, the IP signal can vary whether the current pass through the tissue parallel or perpendicular to the orientation, which can be changed with different electrode placements. However, this effect fades when the current frequency rises and thus is allowed to pass through the capacitive membranes. (Grimnes & Martinsen, 2015)

Bioimpedance consists of two major bodily functions when measured transthoracic, cardiogenic and respiratory part. (Seppä et al. 2011) These signals can give vital information

about both systems. However, when the respiratory system is being evaluated, the cardiogenic signal is considered as interference. It is notable, that the signal does not originate solely from the cardiac and respiratory functions but consists of the effect of multiple tissues in the measurement area. Therefore, the effect of muscle activity on impedance during inspiration has also been studied. (Blanco-Almazán et al. 2019) Consequently to the contribution of chest wall movement, respiratory movement is seen in the impedance signal even if the airway is blocked and the subject only attempts to breathe (Ayad et al. 2019).

Cardiac functions affect the impedance signal through changes in the blood volume in the thorax (Seppä et al. 2011). Blood volume changes according to cardiac cycle, in other words, heartbeat. Due to blood's high water and electrolyte content, blood has a low impedance (Grimnes & Martinsen 2015). As blood volume increases, total impedance decreases (Brown et al. 1994).

The respiratory signal in impedance measurements is originated from the increase in lung volume (Brown et al. 1994). During inspiration, the transthoracic impedance rises and correspondingly it decreases in expiration. The rise in resistance, and thus in impedance, originate from the reduced proportion of electrically conductive matter per volume unit caused by lung dilation in inspiration. (Nopp et al. 1997) In addition, during inspiration and expiration the blood volume is distributed differently in the pulmonary bed (Weng et al. 1979). As the chest cavity expands and deflates the length of the signal path varies also in pace with ventilation (Jeyhani 2017). These variations are seen in the impedance signal, thus enabling the breathing to be analysed with IP.

2.2 Importance of respiration monitoring

Respiratory rate is one of the basic vital signs and is defined as breaths per minute (bpm). In general, 12–20 bpm is considered normal RR (Rolfe, 2019), and is regulated by central nervous system, more precisely the brainstem. The RR is adjusted accordingly to signals from specific mechano- and chemoreceptors monitoring force displacement in lung and chest walls and O_2 and CO_2 levels and pH in the blood. Respiration is induced by muscle contraction of inspiratory muscles, primarily of the diaphragm, creating a negative pressure to the thorax and thus air flow to the lungs. Depth of the breath is determined by muscle contraction as the diaphragm moves substantially more in deep breaths. Whereas the intercostal muscles cause the ribs to flare increasing the volume of the thorax. There are also accessory breathing muscles, like scalene muscles, that are not

active during normal breathing but enhance it if there is a need as during exercise or due to airway obstruction. Expiration, however, is passive in normal breathing, but the abdominal and internal intercostal muscles activate when more efficient breathing is needed. (Koeppen & Stanton 2018)

The gold standard for pulmonary function testing is spirometry. But it has some drawbacks that limit its usability and accuracy. For example, the measuring system partly blocks the airway thus affecting respiration. In addition, the method isn't suitable for ambulatory situations even though it could provide crucial information about patients' condition (Jeyhani, Vuorinen, Noponen et al. 2016) Thus other methods are needed.

All the changes in respiration signal are not linked to respirational problems. As respiration is an important physiological process maintaining the homeostasis, a shift in respiratory rate can be a sign of an imbalance of oxygen or carbon monoxide levels or acid-base balance. When homeostasis is compromised and thus respiration changes, it can be used to predict worsening of the condition. (Rolfe, 2019) Hence more intensive care can be applied earlier and perhaps the most life-threatening conditions can be prevented. Cretikos et al. (2008) list many other severe conditions which have proven to be preceded by a rise in respiration rate. For example, respiration rate significantly rises before cardiac arrest and RR higher than 27 breaths per minute was discovered to be a leading sign before the heart stopped. High respiratory rate is also associated with high mortality rate. (Cretikos et al. 2008)

Other clinically relevant parameters than respiration rate can also be determined from the bioimpedance signals. These parameters are usually defined from the flow curve and the shape of the waveform and tell more about the condition of the lungs. IP measurement is insufficient to measure tidal flow in absolute values as millilitres per second without subject-specific and posture-specific calibration because impedance change ΔZ compared to volume change ΔV is individual and dependent on the position. (Berkebile et al. 2021; Seppä et al. 2013) However, relative parameters do not require absolute values when only the ratio is inspected. The ratio, on the other hand, can be defined from flow or volume waveform shapes which are reproducible from IP measurements. These kinds of parameters include two extensively studied tidal breathing parameters; the ratio of volume at the peak expiratory flow to total expired volume (V_{PTEF}/V_E) and ratio of the

time to reach the tidal peak expiratory flow to total inspiration time (t_{PTEF}/t_E) (Seppä et al. 2010).

Although, with the right placement of the electrodes a linear relationship between ΔZ and ΔV can be obtained, thus enabling flow curve measurements with IP. Seppä et al. (2020) expressed a relationship between decreased expiratory variability index (EVI) and airway obstruction in children. Children's tidal breathing is measured with IP during sleep and the correlation between flow-volume curves is studied. (Seppä et al. 2020) This finding is the basis of a clinical application of Ventica® used for diagnostics of asthma in infants. (Ventica, n.d.) Ventica® proves that IP measurements have clinical value when assessing lung function. A loss of complexity in airflow has also been associated with COPD in adults (Dames et al. 2013). However, regular asthma medication like inhaled corticosteroids can alter the lung function, thus it changes the flow signal and should be noted in the analysis (Seppä et al. 2016).

One challenge with respiration measurements is that the subject's breathing can occur at different depths. The depth of breathing is affected by numerous factors, such as anatomy, obesity, posture and of course due pathological factors. (Seppä et al. 2013) In tidal breathing, the volume of the lungs after the expiration is referred as the functional residual capacity (FRC). If the lung volume falls under FRC, the IP signal is discovered to distort and diminish. (Seppä 2014, p. 58 - 59) Moreover, it is found in studies that patients with higher body mass index (BMI) are more likely to breathe at low lung volumes. Hence, IP might be an insufficient method for measuring respiration changes. (Jones & Nzekwu 2006; Seppä 2014, p. 58–59) However, Młyńczak et al. (2015) found the posture and subject variability to cause more significant variance to the signal than between normal and deep breathing could be seen.

FRC levels are also affected by general anaesthesia making it harder to detect the respiratory functions with IP. Furthermore, the supine position also has a lowering impact on FRC. (Pino & Albrecht 2016, p. 69) In patient monitoring applications, the lack of ability to detect respiratory events during or after anaesthesia is a challenge. Postoperative respiration monitoring is extremely important as opioid-induced ventilatory depression is a significant cause of morbidity and mortality after an operation (Ermer et al. 2019). In a study by Ermer et al. (2019), volunteers were sedated, and low respiratory

rates were measured with different methods. IP did not perform optimally in those conditions, thus more research about using the IP at low RR should be done.

Administered drugs may influence the respiratory functions and therefore must be taken into account when analysing the respiratory signal. Substances like opioids are widely used pain medication and cause respiratory depression as an adverse effect in addition to the analgesic effects by activating special opioid receptors (Hill et al. 2018). Up to 46% of general care floor patients receiving opioids suffered an opioid-induced respiratory depression episode during a 24-hour median monitoring period in a study by Khanna et al. (2020). Patients with ≥1 respiratory depression episodes had approximately 3 days longer hospital stay thus producing more expenses. With continuous respiration monitoring, the incidents could be better predicted and thus the consequences could be diminished. (Khanna et al. 2020)

2.3 Electrodes and their configurations

Electrode locations depend on what is needed from the signal. The magnitude of the impedance caused by the respiratory functions depends highly on the electrode configuration (Jeyhani 2017). Configurations generally aim to optimize one prospect at the expense of other properties. In wearable applications also electrode area can limit the configuration choices. However, a small distance between the electrodes diminishes the respiration-induced impedance changes and thus creates errors (Järvelä et al. 2022).

Bioimpedance is usually measured using either bipolar or tetrapolar electrode configuration. In two-wire measurement, the voltage over the measurement points is sensed through the same wires that are used to feed the current. Consequently, the resistances of the wires and contacts cause voltage drop too, thus the voltage difference between the leads is smaller than it would be across the test resistance alone. This limitation is emphasized if the test resistance is relatively small compared to the resistances of the wires. (Regtien et al. 2004, p.172-173)

In a four-wire system, wire resistances will not cause as significant error as the current is fed through one set of leads, and another set is used for the voltage measurement. In a voltmeter the input impedance is ideally infinite, thus no current flows through voltage sensing leads and therefore no voltage drop occurs in the wires or contacts. In real life, the input impedance is large, but not infinite, hence a small current passes through the

sensing leads causing error in the measurement. (Regtien et al. 2004 p. 172-173) However, the error is substantially smaller than with two electrodes and can usually be neglected. Though four-electrode IP is readily disturbed by motion and can exhibit higher noise levels, it is often the preferred method for IP measurements due to its accuracy (Tuohimäki et al. 2017; Seppä, Pelkonen et al. 2013).

One of the advantages of IP is that the signal can also be gathered with the same electrodes that are used to measure ECG (Jeyhani, 2017). Either standard 12-lead or EASI-configuration can be used for IP. The standard 12-lead ECG consists of six chest electrodes and three limb electrodes on both arms and left leg. The advantage of the EASI system is that it uses fewer electrodes, but the provided signal can be converted into standard 12-lead information. (Jeyhani, Vuorinen, Mäntysalo et al. 2016) Electrode placements for EASI and standard 12-lead configuration are shown in Figure 3.

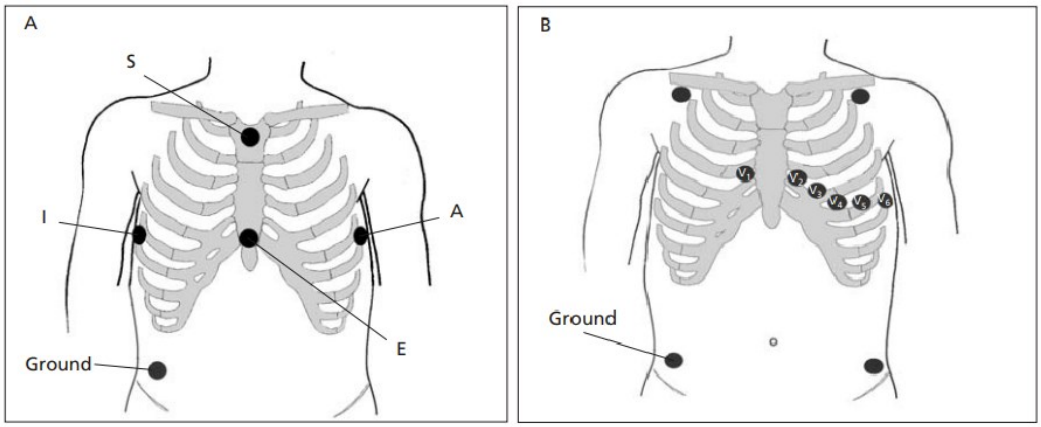

Figure 3. *Electrode locations for A) EASI system and B) Mason-Likar standard 12-lead system. (Welinder et al. 2004)*

In some applications, a small distance between electrodes is needed. Especially in wearable devices this significantly enhances usability. (Jeyhani, Vuorinen, Noponen et al. 2016) One possible placement requiring only a small area is the EAS configuration, a subset of the aforementioned EASI-configuration. The locations of electrodes E, A and S are the lower part of the sternum, V5 of standard ECG and manubrium, respectively. In Jeyhani, Vuorinen, Noponen et al. (2016) study, results show that the most accurate RR and least artefact affected electrode pair for impedance measurements is the S-A lead. In addition, the aforementioned lead also produced the highest amplitudes. Also, measuring the EIP with an electrode patch has been studied. Berkebile et al. (2021) used

a 5.1 cm x 5.1 cm patch located at the sternum to measure not only the respiration rate but also tidal volume with good results. Järvelä et al. (2022) presented a wearable monitoring system using three electrodes. A “dual-vector” method was used to compute the impedance changes as the signal was measured between the chest electrodes and between one chest and the abdominal electrode. The method could detect RR accurately in reference to capnography and tachypnoea recognition was precise. (Järvelä et al. 2022)

Many applications require a high signal-to-motion artifact (SAR) ratio. The optimal electrode configuration with respect to SAR varies with the activity. Lahtinen et al. (2009) presented that placing the electrodes on the flanks resulted in the highest SAR in the sitting position. The same configuration provided also high SAR results when the measurement was done while the patient was running (Lahtinen et al. 2009). High SAR electrode placement could enable the use of IP during sports and everyday life despite its sensitivity to motion artifacts.

High linearity between impedance changes and lung volume changes is also one sought property of IP measurements. Especially when a pulmonary flow curve is to be established, linearity is a desired property. A highly linear relationship is achieved by a four-electrode system, placing the current feeding electrodes on the sides of the thorax whereas the voltage sensing electrodes are on the arms opposing the other electrodes. (Seppä et al. 2013)

Even though placing the electrode around the thorax seems reasonable for respiration monitoring, it is not a necessity. Tavanti et al. (2021) presented a novel configuration of electrodes by placing them around the head. The purpose was to detect the volume changes in the pharynx to obtain the RR. The method was sufficient to establish reliable results also during physical activity. In addition, the electrode placement is suitable for wearable applications and long-term measurements. However, the experiment was performed only on three people, thus more extensive research is required. (Tavanti et al. 2021)

In IP measurements, normal disposable Ag/AgCl electrodes are usually used. While they perform steadily and provide accurate results, these disposable electrodes irritate the

skin and thus are not optimal for long-term applications (Tuohimäki et al. 2017). Therefore, interest towards textile-integrated electrodes has risen. Textile electrodes also improve usability. In the study by Tuohimäki et al. (2017), textile and printed electrodes were compared with regular disposable electrodes in IP and ECG measurements. Especially the textile electrodes performed well regarding noise levels and were able to detect RR adequately. The electrodes were made of medical-grade nylon knit fabric and coated with silver. However, the study was executed only on one person thus wider generalization of the performance of the electrodes with a more extensive group cannot be made based on that study. Nonetheless, the textile electrodes show a promising alternative in long-term applications. (Tuohimäki et al. 2017)

2.4 Processing the respiratory impedance signal

2.4.1 Signal pre-processing

Different types of signal processing methods are needed to get the useful respiratory information from the raw data. However, some basic building blocks are similar in most of the studies. As the signal also contains the cardiogenic oscillation there are options for how to handle it while preserving the respiratory signal.

Distinguishing the cardiogenic and respiratory parts of the signal is based on the fact that within their frequency spectrum most power is at the frequencies of heart rate (HR) and RR, respectively. As the HR is significantly higher than RR, usually at least two times higher, a simple low-pass filter can be used to attenuate the cardiogenic signal. One of this method's drawbacks is that even though a major part of the respiratory signal is in fact at the lower frequencies, it contains also harmonic frequencies that extend to the HR frequencies. Thus, the two signals overlap. While this might not be a big problem when measuring only RR or tidal volume (TV), it is an important factor when measuring more complex parameters. These include for example long-term lung function assessments where valuable variation at higher frequencies could be lost if using a linear low-pass filter. (Seppä et al. 2011) Depending on the chosen RR detection method, the signal might need decimating in which case low-pass filtering is required to prevent aliasing (Fleming & Tarassenko 2007).

Methods to attenuate the cardiogenic oscillations without altering the respiratory signal at higher frequencies have been studied. Consequently, more advanced respiratory parameters can be derived also from IP signal. One way to do this is to process the signal

with Savitzky-Golay (S-G) smoothing filter. While the S-G smoothing filter attenuates the cardiogenic signal, it is able to preserve the high-frequency information at the peaks of the respiration cycle. The performance of the filter is adjusted by finding the optimal frame size. (Seppä et al. 2010) Another method is introduced by Seppä et al. (2011) where a simultaneously measured ECG signal was used to recognize the cardiogenic part of the signal.

Since the IP signal also contains the cardiogenic signal, algorithms for separating the respiratory and cardiac signals have been developed. These can be useful in ambulatory applications where the number of channels for measurements is limited. Thus, it is practical to gather as much physiological information as possible from one signal. (Lu et al. 2019)

2.4.2 Time domain respiration rate algorithms

Respiratory rate detection can be divided into two categories: time domain and frequency domain estimators. (Jeyhani, Vuorinen, Mäntysalo et al. 2016) In the time domain, the signal is analysed in reference to time. Whereas in the frequency domain, the analysis is done in reference to frequency. Moreover, the time domain graph displays how the signal changes over time, but frequency domain graphs present how much of the signal is at a certain frequency range.

Probably the most straightforward method is simple peak detection which is a time domain estimator. In this technique, local maxima are detected and their average distance in seconds was calculated. This value is multiplied by $60/f_s$, where f_s is the sampling frequency. In peak detection, a minimum distance between the maxima must be determined. (Jeyhani, Vuorinen, Mäntysalo et al. 2016) The value sets the maximum RR that can be detected and might vary a little from one research to another which creates deviation in the results. But this limit is usually significantly larger than the frequency of normal breathing. (Jeyhani, Vuorinen, Mäntysalo et al., 2016) Yet there are human-made decisions about the validity of the respiratory functions thus automated detection methods can produce more precise results (Schäfer & Kratky, 2008). The peak detection method performs best if the respiration signal is clear and no distortion is present (Jeyhani, Vuorinen, Mäntysalo et al. 2016).

To eliminate the human decisions about the minimum distance between observations and remove false peak values automated processes based on statistics have been developed. These counting methods define a threshold for defining a valid peak. In the original counting method, first all peaks are detected, and the third quartile of the observations is referred as Q_3 and the threshold is defined as 0.2 x Q_3. A part is considered as a respiration cycle if it fulfils the two following requirements: exactly one minimum below zero without any other extreme values in the region and the cycle starts and ends at maxima above the defined threshold. These strict requirements of the original counting method cause its drawbacks. They lead to ignoring cycles easily thus leaving substantial gaps in the signal. Also, valid respiration cycles are dismissed. (Jeyhani, Vuorinen, Mäntysalo et al. 2016; Schäfer & Kratky 2008)

Schäfer & Kratky (2008) developed the advanced counting method to fix the weaknesses of the original counting method. In advanced counting, the threshold is defined with a similar method to the minimum distance between the maxima. The third quartile of the absolute values of the vertical distances of the minima and maxima multiplied by 0.1 determines the threshold. Next, the pair of maximum and adjacent minimum with the smallest vertical difference is located. If the value is less than the threshold the pair is ignored. Furthermore, this process is iteratively continued until all consecutive maxima and minima are separated by at least the threshold value. With this method, a continuous signal without any gaps is obtained. From both methods, the reciprocal mean of the detected cycle lengths is returned as the RR. (Schäfer & Kratky, 2008)

Another time domain estimator is autocorrelation which is widely used in statistical analysis. To study the periodicity of a signal, the autocorrelation method compares the signal with itself. The autocorrelation function is defined as following

$$r(\tau) = \sum_{n=0}^{N-1-\tau} x(n)x(n+\tau)\,, \tag{7}$$

where $x(n)$ is the signal, *N* the number of samples and τ the lag. Autocorrelation is commonly utilized in medical applications when detecting repeated signal patterns. As the autocorrelation function possesses the same periodic features as the measured signal, the periodic functions of the signal can be examined with the help of the autocorrelation function (Jeyhani, Vuorinen, Mäntysalo et al. 2016). In addition, this method is effective also for eliminating random noise. The RR is obtained from the autocorrelation function,

where the lag of the first peak from the y-axis estimates the cycle length. The lag is then multiplied by $60/f_s$ which results the RR value.

2.4.3 Frequency domain respiration rate algorithms

Moving on to the frequency domain, Fast Fourier Transform (FFT) is widely used in literature to obtain which frequencies the signal contains. When using FFT, the signal is usually decimated to a lower sampling frequency. This step improves the resolution of the spectrum got as a result from the transform to the frequency domain. The RR is obtained from the spectrum as the highest peak in the determined range. (Jeyhani, Vuorinen, Mäntysalo et al. 2016; Tavanti et al. 2021)

Different kinds of autoregressive (AR) models are also used in literature to define RR from the impedance signal. All-pole AR models are statistical prediction models, where a sum of linearly weighted prior observations models the current value. In the frequency domain, poles of the AR model's transfer function determine the spectral peaks. The higher the magnitude of the pole, the higher the magnitude peak in the spectrum is. The phase angle θ of a pole specifies the corresponding frequency *f* of the spectrum peak with the following relationship

$$\theta = 2\pi f \Delta t, \tag{8}$$

where Δt is the sampling interval. To enhance the spectral resolution at low frequencies the signal is decimated to a lower sampling frequency. (Fleming & Tarassenko 2007)

There are different approaches to how a respiration pole can be chosen. Before analysing the respiratory part, poles out of the expected respiration range are excluded (Fleming & Tarassenko 2007). One possibility is to choose the respiration pole with the minimum-angle-pole technique. Before selection, poles with a smaller magnitude than the 95th percentile are discarded. Afterwards, the pole with the smallest angle represents the respiration pole and RR is calculated with Equation 8. (Jeyhani, Vuorinen, Mäntysalo et al. 2016)

An alternative is to determine the RR with the maximum-magnitude-pole method (Jeyhani, Vuorinen, Mäntysalo et al. 2016). Since changes due to respiratory functions are a major component in the signal and other parts are attenuated by filtering, poles

representing the respiratory functions should have high magnitudes (Fleming & Tarassenko 2007). Hence, with this method the pole with the greatest magnitude is chosen to represent the respiration, and frequency is obtained from its phase angle.

AR methods have their assets over FFT. AR models have a continuous spectrum with higher resolution and the signal is more stable for short periods. However, AR is only an estimate whereas FFT is the signal in the frequency domain. Though increasing the model order improves the accuracy of the AR estimate. (Gupta & Mittal 2016) On the other hand, AR models were found to perform poorly if the signal contains higher frequency content either from respiration harmonics or movement artifacts. (Jeyhani, Vuorinen, Mäntysalo et al. 2016)

Even though there are various statistical parameters describing the quality of the processing, the results are not comparable if they use different data sets. In addition, the best-performing algorithm may vary between different electrode configurations and measurement positions. However, in a study that compared all the aforementioned algorithms on IP signal, the advanced counting method performed best compared to others in standing position and during walking. (Jeyhani, Vuorinen, Mäntysalo et al. 2016) Yet many of the studies measuring respiration with IP include a quite small group of subjects (under 20), thus results might vary from one research to another.

Since IP measurements are susceptible to motion artefacts, it would be beneficial to recognize sections with large artifacts or otherwise poor-quality signal from the high-quality regions. These kinds of signal quality indices (SQI) have been studied. SQI proposed by Charlton et al. (2021) assessed the high-quality sections based on the duration of the valid breaths. In the high-quality region, the normalized standard deviation of breath duration should be < 0.25, 85% of the breath durations should be >0.5 or < 1.5 times the median duration and over 60% of the segment should have valid breaths. In addition, individual breaths were compared to the average breath template of the assessed segment. If the mean correlation coefficient was over 0.75 the segment was evaluated as a high-quality segment. However, SQI is not applicable to situations where a RR estimate is needed continuously. (Charlton et al. 2021)

3. RESEARCH METHODOLOGY AND MATERIALS

The research involved five subjects of which 2 males and 3 females. All subjects were informed about the study and written consents were obtained prior to the measurements. The subjects' characteristics are presented in Table 1. All subjects had good general health. The impedance signal was recorded for 2 minutes in the supine position, 2 min in the sitting position and 2 minutes when walking in place. First, the subjects were told to breathe thoracically for 1 min so that in the first half, deep breaths were taken and in the latter part, the breathing was shallower. Then breathing was changed to diaphragmatic and the same variation in depth of the breathing was applied. The same breathing protocol was repeated in all positions with two different electrode placements.

Table 1. *Subjects' characteristics*

	Mean ± standard deviation	*Range*
Age (years)	26.6 ± 9.0	21–42
Height (cm)	168.6 ± 7.2	162–79
Weight (kg)	70.0 ± 12.9	58–90
Body mass index	24.5 ± 3.4	22.0–30.1

The electrodes were first positioned on Mason-Likar (M-L) arm electrode locations and secondly at the V5 location of the standard 12-lead system and the corresponding placement on the right side. The electrodes used in the measurement were Ambu® BlueSensor L (L-00-S/25) electrodes, disposable standard Ag/AgCl electrodes with electrolyte gel to minimize the skin-electrode resistance.

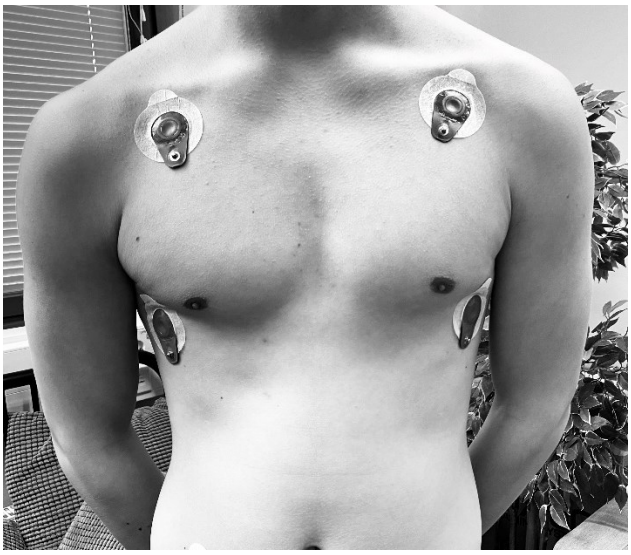

Figure 4. *Electrode locations, upper ones referred as M-L electrodes and the lower ones V5 electrodes*

The respiration was measured with two devices simultaneously. The IP data acquisition was done with Biopac EBI100C device. A test current of 400 μA with a frequency of 50 kHz was used. The build-in filters of the Biopac device were used with a passband from 0.05 Hz to 100 Hz. For the acquisition of signal, the sampling frequency was 500 samples per second. Secondly, a pneumotachograph (PNT) was used to collect a reference signal for the evaluation of the IP data.

All signal processing was done in the MATLAB2022A program. Before running the respiration rate algorithms, the raw IP data was processed with a direct-form FIR lowpass filter with 0.6167 Hz stop-band frequency. Both IP and PNT volume data were filtered with 3rd order Butterworth high-pass filter with 0.06 Hz cut-off frequency to remove baseline wandering. The IP volume signal was multiplied with a calibration factor which was calculated from a ratio of median breath volume in PNT and in IP. The respiration rates were detected with peak detection, advanced counting and FFT method. With peak detection, the criterion was to have a minimum horizontal distance of 1.5 s, corresponding to 40 bpm. Before performing the FFT, the signal was filtered with 3rd order Butterworth filter with a cut-off frequency of 2 Hz to avoid aliasing as the signal was decimated to 4 samples per second. For further analysis of the algorithms, the mean absolute error (MAE) and mean absolute percentage error (MAPE) were calculated from the signal. The MAE is defined as

$$MAE = \frac{1}{N}\sum_{n=1}^{N}|\hat{y}[n] - y[n]| \tag{9}$$

and MAPE

$$MAPE = \frac{1}{N}\sum_{n=1}^{N}\left|\frac{\hat{y}[n] - y[n]}{y[n]}\right| \cdot 100\ \%, \tag{10}$$

where $\hat{y}[n]$ is the RR estimate from the IP signal and $y[n]$ the RR from the reference. The final results were rounded up to prevent underestimation of the error.

4. RESULTS AND ANALYSIS

The signal quality in different postures is assessed from the figures of the measured respiration signal over time. Figures that illustrate the conclusions are presented in the text and the figures of complete measurement of each subject can be found in Appendix A. For further analysis of the effect of posture and performance of RR detection algorithms, the average RR in each posture is obtained with 3 algorithms and MAE and MAPE of the estimates are calculated. The MAE and MAPE results with M-L arm electrodes are presented in Table 2 and Table 3, respectively and corresponding values with V5 electrodes in Table 4 and Table 5.

Table 2. *MAE results with M-L arm electrodes*

	Supine (bpm)	*Sitting (bpm)*	*Walking (bpm)*	*Total (bpm)*
Peak detection	0,32	1,23	1,49	1,01
Advanced counting	0,44	2,28	3,28	2,00
FFT	0,05	2,63	0,19	0,96

Table 3. *MAPE results with M-L arm electrodes*

	Supine (%)	*Sitting (%)*	*Walking (%)*	*Total (%)*
Peak detection	2,83	7,23	6,92	5,65
Advanced counting	2,96	12,83	15,71	10,50
FFT	0,47	20,14	1,50	7,37

Table 4. *MAE results with V5 electrodes*

	Supine (bpm)	*Sitting (bpm)*	*Walking (bpm)*	*Total (bpm)*
Peak detection	0,63	1,03	0,97	0,88
Advanced counting	1,47	2,08	2,52	2,42
FFT	0,38	1,93	0,15	0,82

Table 5. *MAPE results with V5 electrodes*

	Supine (%)	*Sitting (%)*	*Walking (%)*	*Total (%)*
Peak detection	3,78	8,07	5,36	5,74
Advanced counting	7,42	9,40	11,58	9,47
FFT	3,73	12,93	1,27	5,98

4.1 Time-domain analysis of signal quality

The quality of the signal varied notably between subjects and measurement phases. The subject's posture was changed after phase 2 and phase 4. The amount and magnitude of motion artefacts ranged from hardly noticeable (Figure 5) to vastly distorting (Figure 6). Subject 4 tried also to improve position during phase 4 in Figure 6, which can be seen as large motion artefacts. During the walking phase, the filtering removed quite successfully the motion artefacts as the frequency of walking is mostly out of the frequency range of respiration. Thus, the respiration signal was readable especially when deeper breaths were taken. Parts with shallower breathing were more sensitive to distortions which can be seen in Figure 6.

The presented figures are divided into six phases corresponding to the following performance

1. Supine position, thoracic breathing
2. Supine position, diaphragmatic breathing
3. Sitting, thoracic breathing
4. Sitting, diaphragmatic breathing
5. Walking stationary, thoracic breathing
6. Walking stationary, diaphragmatic breathing.

Within each phase, the first half represents deep breaths and the latter half shallow breaths.

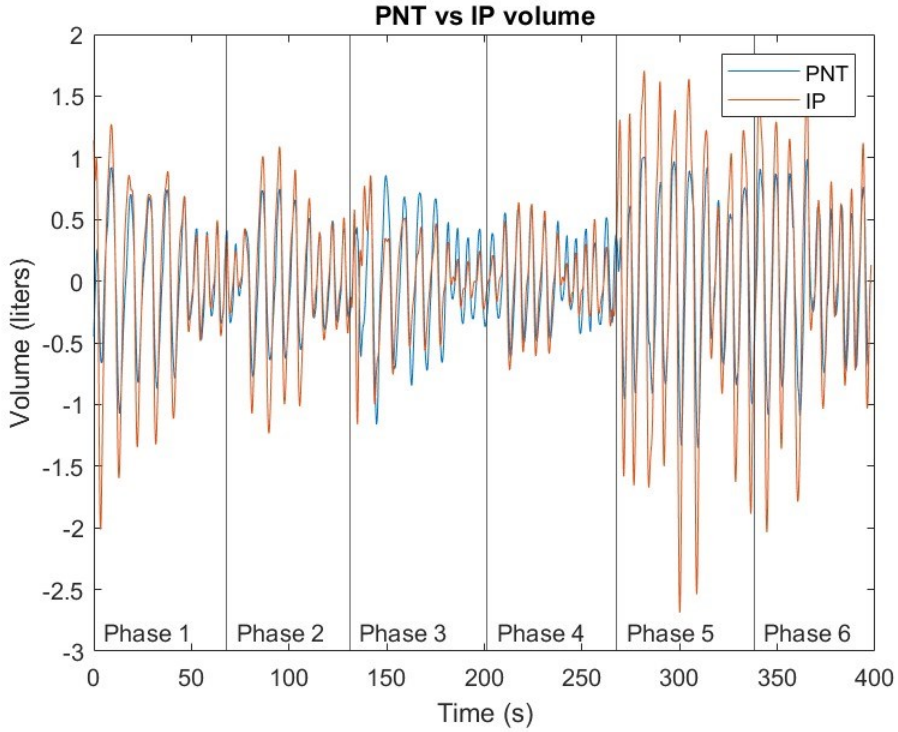

Figure 5. *Breathing volume signal (blue) and corresponding amplitude scaled IP signal (red) of subject 5 measured with V5 electrodes*

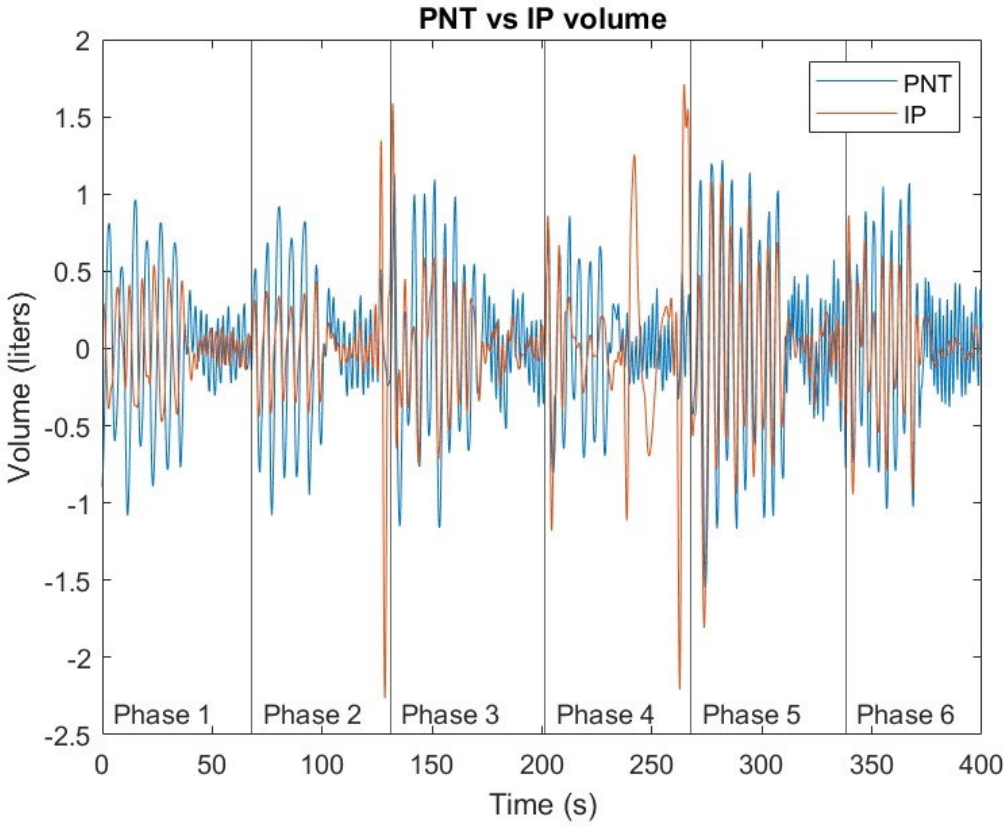

Figure 6. *Breathing volume signal (blue) and corresponding amplitude scaled IP signal (red) of subject 4 with M-L arm electrodes*

No recurring or clear changes between thoracic and diaphragmatic breathing patterns were seen. This may be also affected by the difficulty of maintaining thoracic or diaphragmatic breathing throughout the whole measurement period. Neither the breathing depth was controlled which might explain why all measurements did not show as clear variation in the amplitude of the PNT-derived volume signal. However, with some subjects the amplitudes of the breath volume signal from IP were especially low in the region of the diaphragmatic breathing phase in the sitting position making the breaths harder to detect. This is illustrated in Figure 7, where phase 4 represents diaphragmatic breathing in the sitting position. In general, the periods of shallow breathing were noisier, and detection of individual breaths was harder, which can be seen for example in Figure 8.

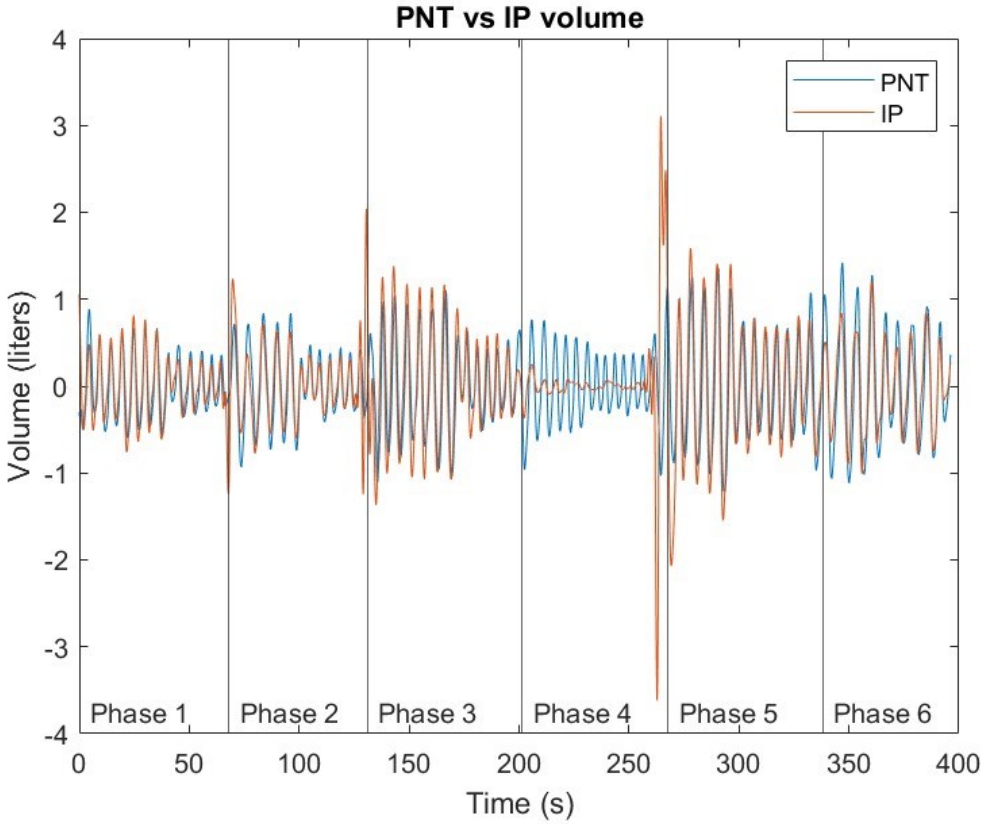

Figure 7. *Breathing volume signal (blue) and corresponding amplitude scaled IP signal (red) of subject 1 with M-L arm electrodes*

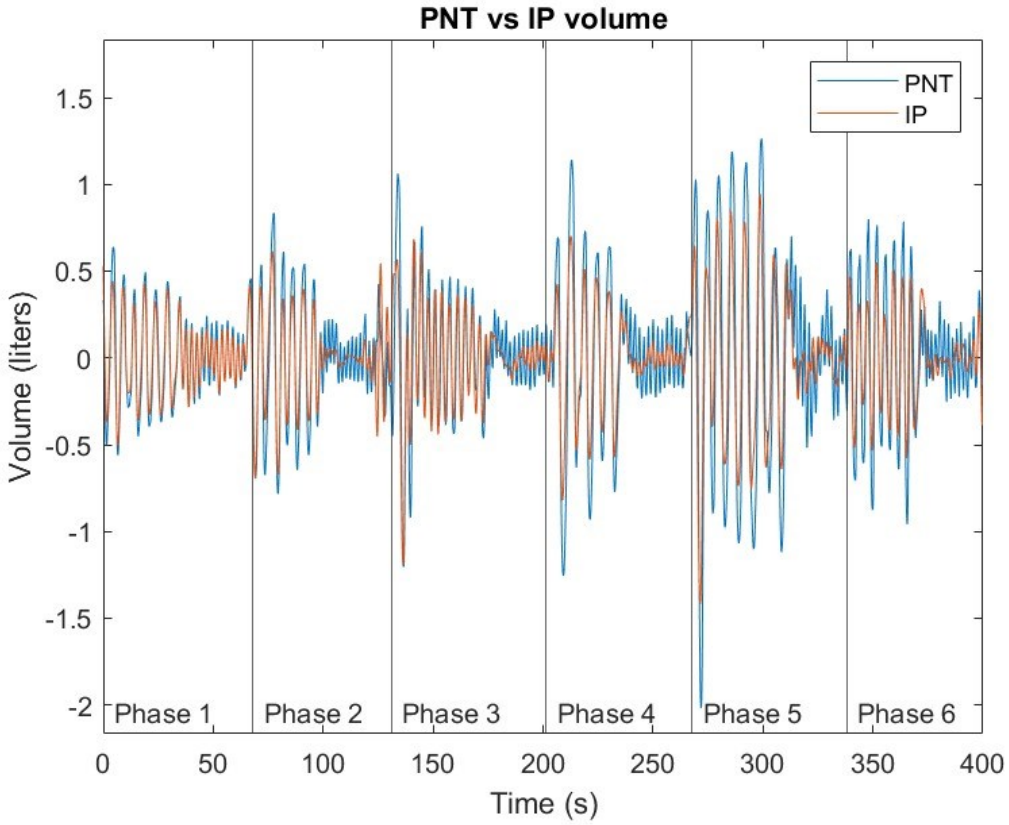

Figure 8. *Breathing volume signal (blue) and corresponding amplitude scaled IP signal (red) of subject 4 with V5 electrodes*

Figures 5–7 illustrate how the performance of the calibration factor varied. In Figure 7, the volume of the IP signal agrees reasonably well with the reference volume at some parts of the measurement. Whereas in Figure 6, the IP signal fails to produce reliable estimates of the breath volumes. For time-domain analysis, the calibration factor was calculated from the whole data. If the ratio of PNT and IP amplitudes would remain constant throughout the measurement, the calibration factor should have functioned better converting IP signal to volume. Hence, it can be stated that IP amplitude is not linearly dependent on the lung volume with either electrode configuration. However, the electrode configurations used in this study did not aim for linearity but reliable RR detection and incomplete calibration did not preclude the RR detection.

With subject 4, a substantial phase shift was obtained in the IP signal compared to the reference. However, as the measurement proceeds, the phase shift seems to normalize and the volume changes in IP and reference are simultaneous. The situation is presented in Figure 9. The cause of the phase shift is unclear and a similar phenomenon does not occur in other measurements. Further studies could include determining the prevalence and origin of the phase shift.

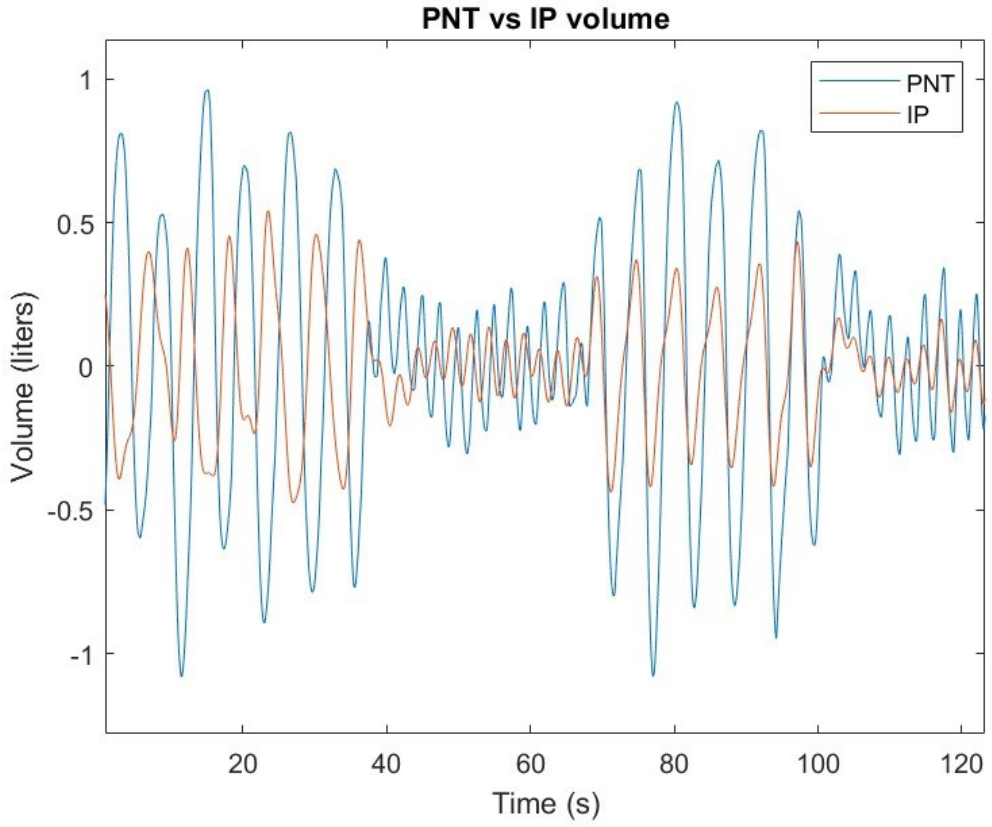

Figure 9. *Breath volume signal (blue) and corresponding amplitude scaled IP signal (red) of subject 4 in supine position with M-L arm electrodes*

The study did not include periods of natural breathing. In any case, completely natural breathing is hard to maintain as concentrating on one's breathing can cause an alteration in breathing pattern. In addition, PNT as a reference method is problematic. Using a mask partially obstructs the airway, hence the breathing can be disturbed. Some airflow can pass also through the nose. However, reference is essential to reliably assess the performance of the technique and RR detection algorithms.

4.2 Performance of algorithms

For respiration rate detection, the data was divided into three parts according to subject postures. Thus, the parts with motion artefacts from changing the posture were excluded from the calculations. Manual exclusion of motion artefacts affects positively MAE and MAPE results but diminishes their applicability to continuous measurements. In continuous measurements, the motion artefacts would cause unreliableness to the results which would have to be considered in practical solutions. However, the removal of low-signal quality sections is somewhat comparable to the operation of SQI (Charlton et al. 2021).

There is no gold standard algorithm for respiration detections, thus establishing the real RR is a challenge. Therefore, the RR estimate from the IP signal is compared to the reference processed with the same algorithm. This procedure might lead to inaccurate MAE and MAPE results if the algorithm is unable to successfully detect the RR from the reference, which was the case with the FFT.

With the FFT algorithm, the RR estimates agreed well with those from the reference signal. Even though the MAE values were smallest with FFT method, the estimates differed considerably from manually estimated respiration rates. Thus, the method is excluded from further comparison with other algorithms. Significant errors were probably caused by unsuitable window length for this specific method. The data was divided into roughly 2-minute sections and the spectrum is calculated for the whole section, where the highest maximum was reported as respiration frequency. In reality, the RR does not stay constant but varies during the measurement period consequently the power from the respiration signal is divided to a wider range of frequencies. Thus, only one estimate from the 2-minute period does not reliably illustrate the real situation. In practical applications, a moving window with a smaller window length is used to get results from a wider range of frequencies. Small MAE results indicate that the algorithm could perform relatively well at least with a clean signal if smaller moving window would be used. However, this requires further research.

When considering the other two algorithms, peak detection performed better than advanced counting with both electrode configurations in this study. These results are contrary to the findings of Jeyhani, Vuorinen, Mäntysalo et al. (2016), though they did not include breathing at different depths. Considering advanced counting, variation in depth of the breaths possibly set the threshold for vertical distances too high, hence small breaths in poor signal quality sections were readily missed. However, if the signal was clean with minimal distortions MAE scores similar to peak detection were observed also with advanced counting. The performance of the advanced counting method could be improved in the future by developing an adaptive threshold that would recognize the variation of depth but would still be able to filter out random fluctuations.

For example, in Figure 10, a long period without detected breaths is seen. Since the RR is calculated as an average of breathing cycle lengths, large blind areas can have a

major effect on the results especially when the measurement period is relatively short. The corresponding signal part processed with the peak detection algorithm is shown in Figure 11. On the contrary, the peak detection method does recognize breaths from the region where advanced counting failed, but there are also wrongly detected peaks. It is hard to distinguish if any of the variations between 80 and 120 seconds is respiration related, hence the peak detection algorithm performs almost as poorly as advanced counting in this region.

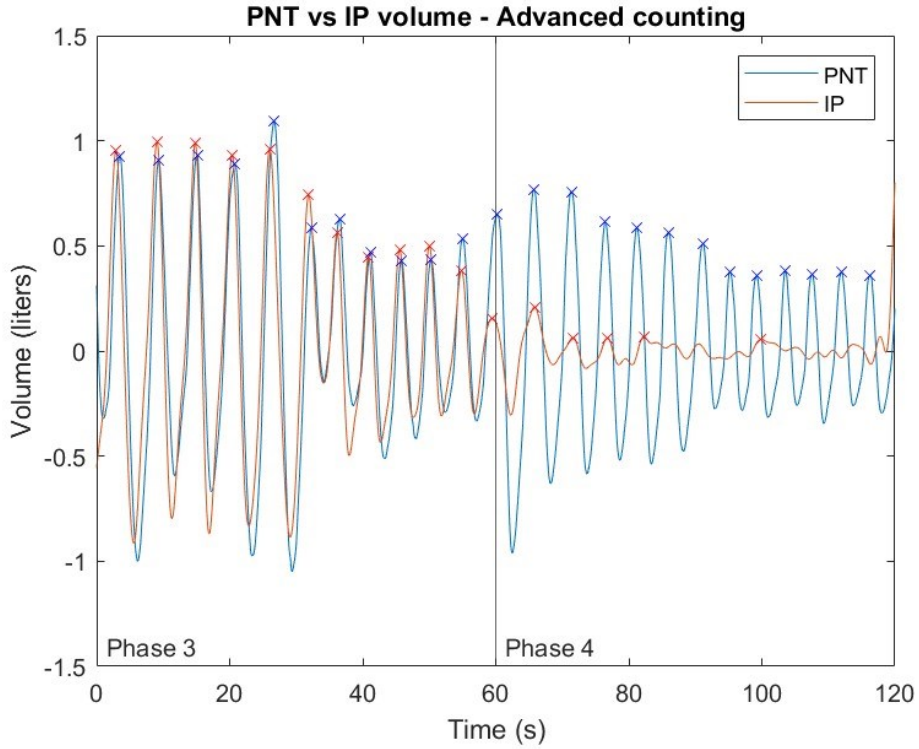

Figure 10. *Breath volume signal (blue) and corresponding amplitude scaled IP signal (red) of subject 1 in sitting posture with M-L electrodes processed with advanced counting*

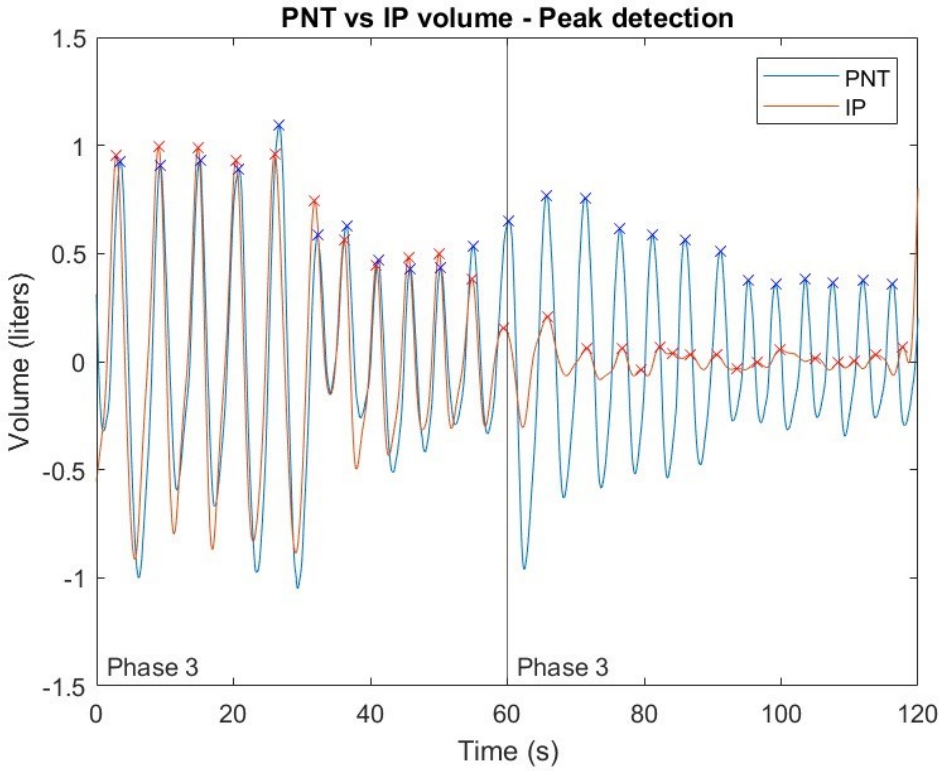

Figure 11. *Breath volume signal (blue) and corresponding amplitude scaled IP signal (red) of subject 1 in sitting posture with M-L electrodes processed with peak detection*

Tables 2-5 show that both algorithms were able to detect the RR most accurately when the subject was in the supine position. It is notable from tables 2 and 3, that the MAPE of the walking phase is smaller than that of the sitting phase whereas the MAE is greater with the walking phase. However, some of this effect is explained by the decrease in the ratio of error and reference when the RR rose during the walking phase with some subjects.

4.3 Effect of electrode configuration

From tables 2–5 can be seen, that with M-L electrodes, the MAE seems to rise when subjects rose whereas with V5 electrodes the position does not seem to have as significant effect. These results indicate that M-L electrodes would be more optimal choice for IP measurement on stationary people, like patients in bed care, whereas electrodes in V5 locations would perform better in portable applications measuring more active subjects. However, this study had a quite small sample size and noisy signals were obtained quite equally from both configurations. With more extensive study, the effect of random

fluctuations might be smaller and clearer differences between electrode configurations could be seen.

Separate measurements with different electrode configurations complicate the comparison of results. Conclusions about the performance of the configuration cannot be reliably made from a noisy signal from either configuration as a reference signal from the other location was not obtained simultaneously. However, concurrent measurements are challenging with active techniques like IP as current fed from the other electrode pair could affect the signal measured from the other electrodes.

It can also be questioned if the electrodes stayed stationary throughout the measurement period while long wires to connect the electrodes and measurement device moved. The slightest movement in electrode positions would cause significant noise. At least with subject 4, the other adhesive surface of the V5 electrodes was slightly loosened and the signal was quite noisy, especially during shallow breathing. Also, the Biopac EBI100C device has default connections for 4-wire measurements. Hence, some modifications to the electrode wiring had to be done. It is possible that the assembly was loose, and the connections were occasionally able to move generating noise to the signal.

The influence of sex or BMI was not considered in this study as the sample size was relatively small. Subject-specific characteristics can affect the performance of the IP and future studies could examine if certain electrode configuration functions better with specific characteristics. However, a general electrode configuration would be better considering the functionality, especially in the patient monitoring applications.

5. CONCLUSIONS

The objective of this study was to assess the effects of position and electrode configuration on the respiration signal measured with the bioimpedance technique. Also, the influence of thoracic and diaphragmatic breathing at different depths was considered. Average respiration rates were calculated in different positions with three algorithms and their performance was evaluated. The results were compared with the reference signal obtained from a pneumotachometer. The sample size was quite small, hence broad generalizations of the effects cannot be reliably made but the study provides indicative results for the objects.

Bioimpedance signals are easily disturbed by motion and the results comply with that as the signal was clearest in the supine position. The performance of the algorithms varied, but simple peak detection produced the most reliable results in this research setting. The window length was too long to obtain reasonable RR estimates. The advanced counting method provided relatively good results on clear data but the detection of shallow breaths from noisy signal was a challenge. Thoracic and diaphragmatic breathing did not cause significant differences in the signal.

Conclusions about the effect of electrode configuration are challenging to make as the measurements were not performed simultaneously. Neither configuration appeared clearly superior to another, but noisy and clean signal was obtained equally with both electrode configurations. The most accurate RR estimates were obtained in the supine position with M-L arm electrodes. However, the results imply that the position does not have as significant effect on signal measured with V5 configuration.

In many studies, the presented study included, the subjects have been relatively young and had good general health. If patient monitor application is considered, these characteristics do not necessarily represent the most abundant user base. Therefore, the performance of the method might be exaggerated. Thus, future research should include subjects with a wider range of characteristics. There is clear evidence that respiration rate is an important predictor of deterioration of the patient's condition. Impedance pneumography offers an unobtrusive and simple way to improve the monitoring of currently poorly utilized vital sign.

REFERENCES

AL-Khalidi, F. Q., Saatchi, R., Burke, D., Elphick, H. & Tan, S. (2011) Respiration Rate Monitoring Methods: A Review. *Pediatric pulmonology*, 46 (6), pp. 523–529.

Ayad, S., Khanna, A. K., Iqbal, S. U. & Singla, N. (2019) Characterisation and Monitoring of Postoperative Respiratory Depression: Current Approaches and Future Considerations. *British journal of anaesthesia : BJA*, 123 (3), pp. 378–391.

Berkebile, J. A., Mabrouk, S., Ganti, V., Srivatsa, A., Sanchez-Perez, J. & Inan, O. (2021) Towards Estimation of Tidal Volume and Respiratory Timings via Wearable-Patch-Based Impedance Pneumography in Ambulatory Settings. *IEEE Transactions on Biomedical Engineering*.

Blanco-Almazán, D., Groenendaal, W., Catthoor, F. & Jané, R. (2019) Chest Movement and Respiratory Volume Both Contribute to Thoracic Bioimpedance during Loaded Breathing. *Scientific reports*, 9 (1), pp. 20232–11.

Brown, B. H., Barber, D. C., Morice, A. H. & Leathard, A. D. (1994) Cardiac and Respiratory Related Electrical Impedance Changes in the Human Thorax. *IEEE Transactions on Biomedical Engineering*, 41 (8), pp. 729–734.

Charlton, P. H., Bonnici, T., Tarassenko, L., Clifton, D. A., Beale, R., Watkinson, P. J. & Alastruey, J. (2021) An Impedance Pneumography Signal Quality Index: Design, Assessment and Application to Respiratory Rate Monitoring. *Biomedical signal processing and control*, 65, pp. 102339–102339.

Cretikos, M. A., Bellomo, R., Hillman, K., Chen, J., Finfer, S. & Flabouris, A. (2008) Respiratory Rate: The Neglected Vital Sign. *Medical journal of Australia*, 188 (11), pp. 657–659.

Dames, K. K., Lopes, A. J. & Melo, P. L. de (2013) Airflow Pattern Complexity during Resting Breathing in Patients with COPD: Effect of Airway Obstruction. *Respiratory physiology & neurobiology*, 192, pp. 39–47.

Ermer, S., Brewer, L., Orr, J., Egan, T. D. & Johnson, K. (2019) Comparison of 7 Different Sensors for Detecting Low Respiratory Rates Using a Single Breath Detection Algorithm in Nonintubated, Sedated Volunteers. *Anesthesia and analgesia*, 129 (2), pp. 399–408.

Fleming, S. G. & Tarassenko, L. (2007) A Comparison of Signal Processing Techniques for the Extraction of Breathing Rate from the Photoplethysmogram. *Int. J. Biol. Med. Sci*, 2 (4), pp. 232–236.

Grimnes, S. & Martinsen, Ø. G. (2015) *Bioimpedance and Bioelectricity Basics*. London, England: Academic Press.

Gupta, V. & Mittal, M. (2016) Respiratory Signal Analysis Using PCA, FFT and ARTFA. In: *2016 International Conference on Electrical Power and Energy Systems (ICEPES)*, *2016*. IEEE, pp. 221–225.

Hill, R., Disney, A., Conibear, A., Sutcliffe, K., Dewey, W., Husbands, S., Bailey, C., Kelly, E. & Henderson, G. (2018) The Novel M-opioid Receptor Agonist PZM21 Depresses Respiration and Induces Tolerance to Antinociception. *British journal of pharmacology*, 175 (13), pp. 2653–2661.

Järvelä, K., Takala, P., Michard, F. & Vikatmaa, L. (2022) Clinical Evaluation of a Wearable Sensor for Mobile Monitoring of Respiratory Rate on Hospital Wards. *Journal of Clinical Monitoring and Computing* [Online], 36 (1) February, pp. 81–86. Available from: <https://link.springer.com/article/10.1007/s10877-021-00753-6> [Accessed 3 April 2022].

Jeyhani, V. (2017) A Wireless Device for Ambulatory Cardiac and Respiratory Monitoring - Design Considerations and Essential Performance.

Jeyhani, V., Vuorinen, T., Mäntysalo, M. & Vehkaoja, A. (2016) Comparison of Simple Algorithms for Estimating Respiration Rate from Electrical Impedance Pneumography Signals in Wearable Devices. *Health and technology*, 7 (1), pp. 21–31.

Jeyhani, V., Vuorinen, T., Noponen, K., Mäntysalo, M. & Vehkaoja, A. (2016) Optimal Short Distance Electrode Locations for Impedance Pneumography Measurement from the Frontal Thoracic Area. Springer Verlag.

Jones, R. L. & Nzekwu, M.-M. U. (2006) The Effects of Body Mass Index on Lung Volumes. *Chest*, 130 (3), pp. 827–833.

Khalil, S. F., Mohktar, M. S. & Ibrahim, F. (2014) The Theory and Fundamentals of Bioimpedance Analysis in Clinical Status Monitoring and Diagnosis of Diseases. *Sensors (Basel, Switzerland)* [Online], 14 (6) June, pp. 10895–10928. Available from: <https://pubmed.ncbi.nlm.nih.gov/24949644>.

Khanna, A. K., Bergese, S. D., Jungquist, C. R., Morimatsu, H., Uezono, S., Lee, S., … & Overdyk, F. J. (2020) Prediction of Opioid-Induced Respiratory Depression on Inpatient Wards Using Continuous Capnography and Oximetry: An International Prospective, Observational Trial. *Anesthesia and Analgesia* [Online], pp. 1012–1024. Available from: <https://journals.lww.com/anesthesia-analgesia/Fulltext/2020/10000/Prediction_of_Opioid_Induced_Respiratory.6.aspx> [Accessed 4 April 2022].

Koeppen, B. M. & Stanton, B. A. (2018) *Berne & Levy Physiology*. Philadelphia, PA: Elsevier.

Lahtinen, O., Seppä, V.-P., Väisänen, J. & Hyttinen, J. (2009) Optimal Electrode Configurations for Impedance Pneumography during Sports Activities. In: Sloten, J. vander, Verdonck, P., Nyssen, M. & Haueisen, J. ed., *4th European Conference of the International Federation for Medical and Biological Engineering*, *2009*. Berlin, Heidelberg: Springer Berlin Heidelberg, pp. 1750–1753.

Lu, Y., Wu, H. & Malik, J. (2019) Recycling Cardiogenic Artifacts in Impedance Pneumography. *Biomedical signal processing and control*, 51, pp. 162–170.

Mansfield, M. (2011) Understanding Physics. Chichester, West Sussex: Wiley.

Mlynczak, M. & Cybulski, G. (2017) Decomposition of the Cardiac and Respiratory Components from Impedance Pneumography Signals. In: *BIOSIGNALS*, *2017*. pp. 26–33.

Młyńczak, M., Niewiadomski, W., Żyliński, M. & Cybulski, G. (2015) Verification of the Respiratory Parameters Derived from Impedance Pneumography during Normal and Deep Breathing in Three Body Postures. In: *6th European Conference of the International Federation for Medical and Biological Engineering*. Cham: Springer International Publishing, pp. 881–884.

Nopp, P., Harris, N. D., Zhao, T.-X. & Brown, B. H. (1997) Model for the Dielectric Properties of Human Lung Tissue against Frequency and Air Content. *Medical & biological engineering & computing*, 35 (6), pp. 695–702.

Pino, R. M. & Albrecht, M. A. (2016) *Handbook of Clinical Anesthesia Procedures of the Massachusetts General Hospital*. Philadelphia: Wolters Kluwer.

Regtien, P., Heijden, F. van der, Korsten, M. J. & Otthius, W. (2004) *Measurement Science for Engineers*. Jordan Hill: Elsevier Science & Technology.

Rolfe, S. (2019) The Importance of Respiratory Rate Monitoring. *British Journal of Nursing* [Online], 28 (8), pp. 504–508. Available from: <https://doi.org/10.12968/bjon.2019.28.8.504>.

Schäfer, A. & Kratky, K. W. (2008) Estimation of Breathing Rate from Respiratory Sinus Arrhythmia: Comparison of Various Methods. *Annals of biomedical engineering*, 36 (3), pp. 476–485.

Seppä, V. P., Hyttinen, J. & Viik, J. (2011) A Method for Suppressing Cardiogenic Oscillationsin Impedance Pneumography. *Physiological Measurement*, 32 (3), pp. 337–345.

Seppä, V. P., Pelkonen, A. S., Kotaniemi-Syrjänen, A., Viik, J., Mäkelä, M. J. & Malmberg, L. P. (2016) Tidal Flow Variability Measured by Impedance Pneumography Relates to Childhood Asthma Risk. *European Respiratory Journal* [Online], 47 (6) June, pp. 1687–1696. Available from: <https://erj.ersjournals.com/content/47/6/1687> [Accessed 23 March 2022].

Seppä, V. P., Viik, J. & Hyttinen, J. (2010) Assessment of Pulmonary Flow Using Impedance Pneumography. *IEEE Transactions on Biomedical Engineering*, 57 (9) September, pp. 2277–2285.

Seppä, V.-P. (2014) Development and Clinical Application of Impedance Pneumography Technique. Tampere University of Technology.

Seppä, V.-P., Gracia-Tabuenca, J., Kotaniemi-Syrjänen, A., Malmström, K., Hult, A., Pelkonen, A. S., Mäkelä, M. J., Viik, J. & Malmberg, L. P. (2020) Expiratory Variability Index Is Associated with Asthma Risk, Wheeze and Lung Function in Infants with Recurrent Respiratory Symptoms. *ERJ open research*, 6 (4), p. 167.

Seppä, V.-P., Hyttinen, J., Uitto, M., Chrapek, W. & Viik, J. (2013) Novel Electrode Configuration for Highly Linear Impedance Pneumography. *Biomedizinische Technik*, 58 (1), pp. 35–38.

Tavanti, E., Gambari, G., Boero, F., Fedeli, A., Pastorino, M. & Randazzo, A. (2021) A Breath Monitoring Approach Based on Electrical Impedance Measurements. *IEEE journal of electromagnetics, RF and microwaves in medicine and biology*, 5 (2), pp. 179–186.

Tuohimäki, K., Mahdiani, S., Jeyhani, V., Vehkaoja, A., Iso-Ketola, P., Vanhala, J., Viik, J. & Mäntysalo, M. (2017) Electrode Comparison for Textile-Integrated Electrocardiogram and Impedance Pneumography Measurement. Springer Verlag.

Ventica (n.d.) *Expiration Variability Index EVI - Ventica* [Online]. Ventica. Available from: <https://www.ventica.net/expiration-variability-index-evi/> [Accessed 20 March 2022].

Ville-Pekka Seppä, Anna S. Pelkonen, Anne Kotaniemi-Syrjänen, Mika J. Mäkelä, Jari Viik & L. Pekka Malmberg (2013) Tidal Breathing Flow Measurement in Awake Young Children by Using Impedance Pneumography. *Journal of Applied Physiology*, 115 (11), pp. 1725–1731.

Welinder, A., Sörnmo, L., Feild, D. Q., Feldman, C. L., Pettersson, J., Wagner, G. S. & Pahlm, O. (2004) Comparison of Signal Quality between EASI and Mason-Likar 12-Lead Electrocardiograms during Physical Activity. *American journal of critical care*, 13 (3), pp. 228–234.

Weng, T. R., Spence, J. A., Polgar, G. & Nyboer, J. (1979) Measurement of Regional Lung Function by Tetrapolar Electrical Impedance Plethysmography. *Chest*, 76 (1), pp. 64–69.

APPENDIX A: COMPLETE COLLECTION OF BREATH VOLUME GRAPHS

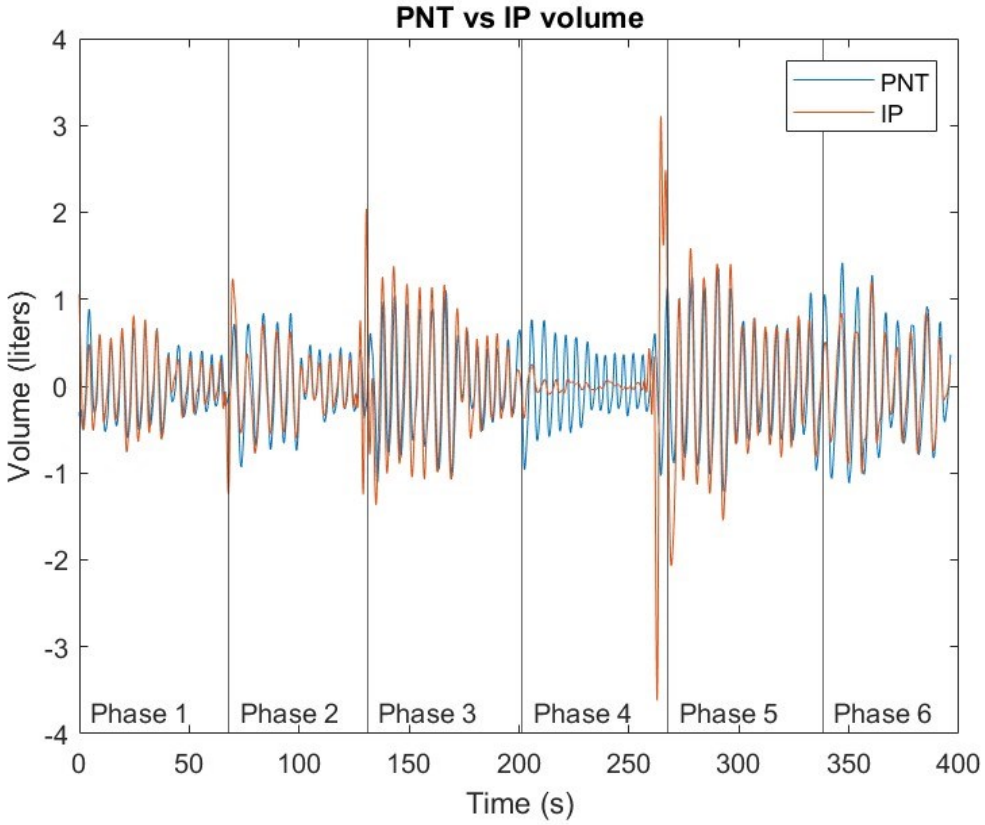

Figure 12. *Breath volume signal (blue) and corresponding amplitude scaled IP signal (red) of subject 1 with Mason-Likar arm electrodes*

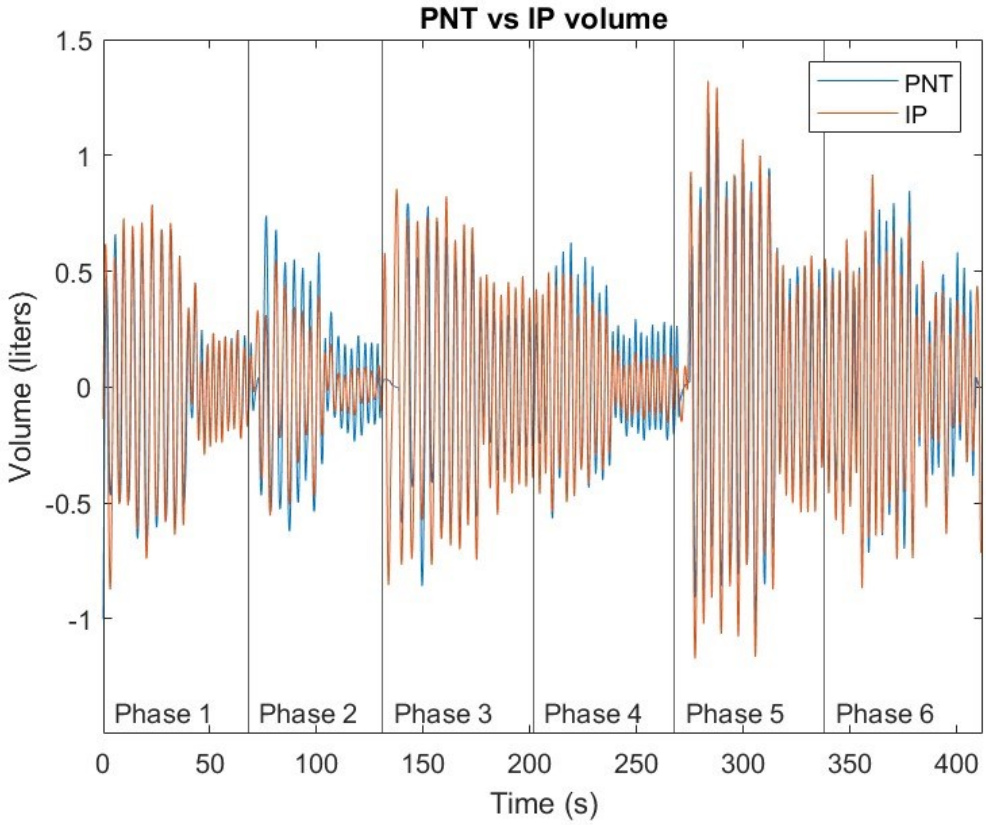

Figure 13. *Breath volume signal (blue) and corresponding amplitude scaled IP signal (red) of subject 2 with Mason-Likar arm electrodes*

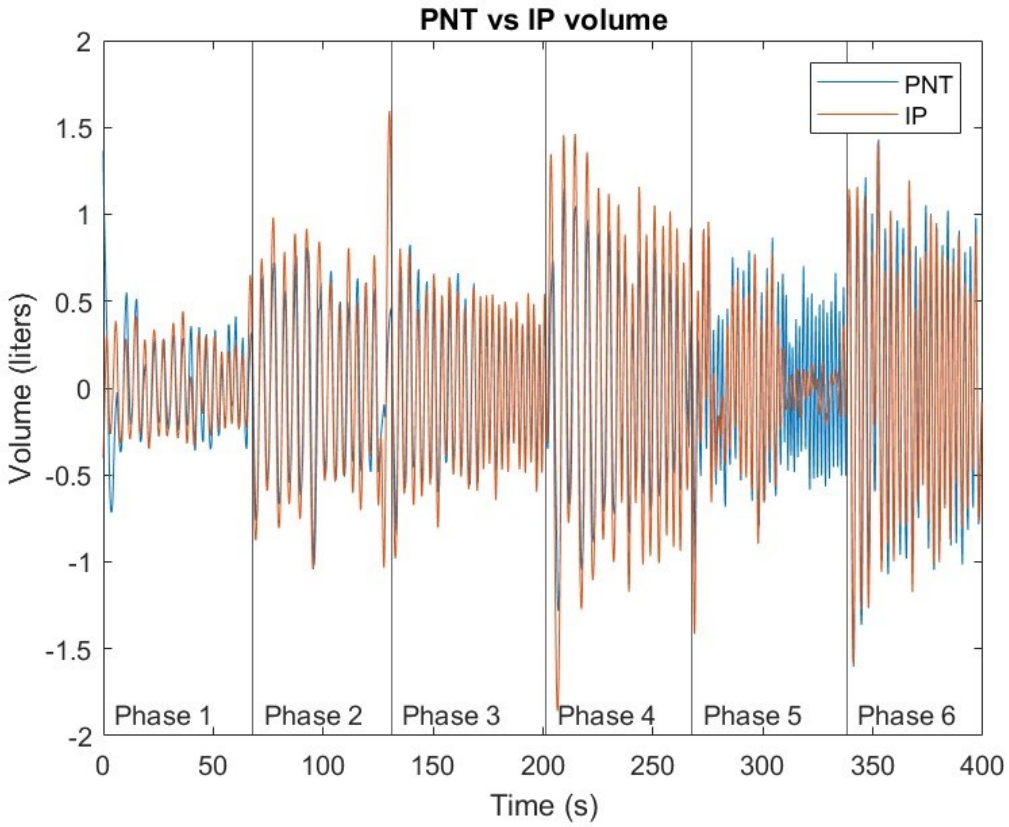

Figure 14. *Breath volume signal (blue) and corresponding amplitude scaled IP signal (red) of subject 3 with Mason-Likar arm electrodes*

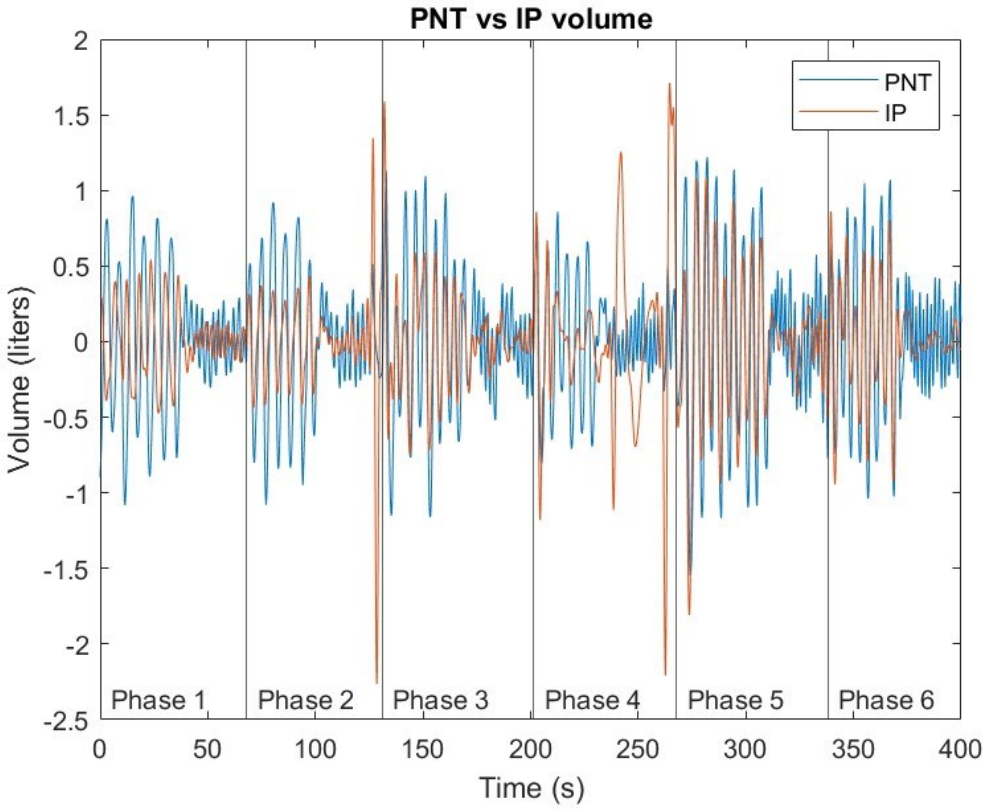

Figure 15. *Breath volume signal (blue) and corresponding amplitude scaled IP signal (red) of subject 4 with Mason-Likar arm electrodes*

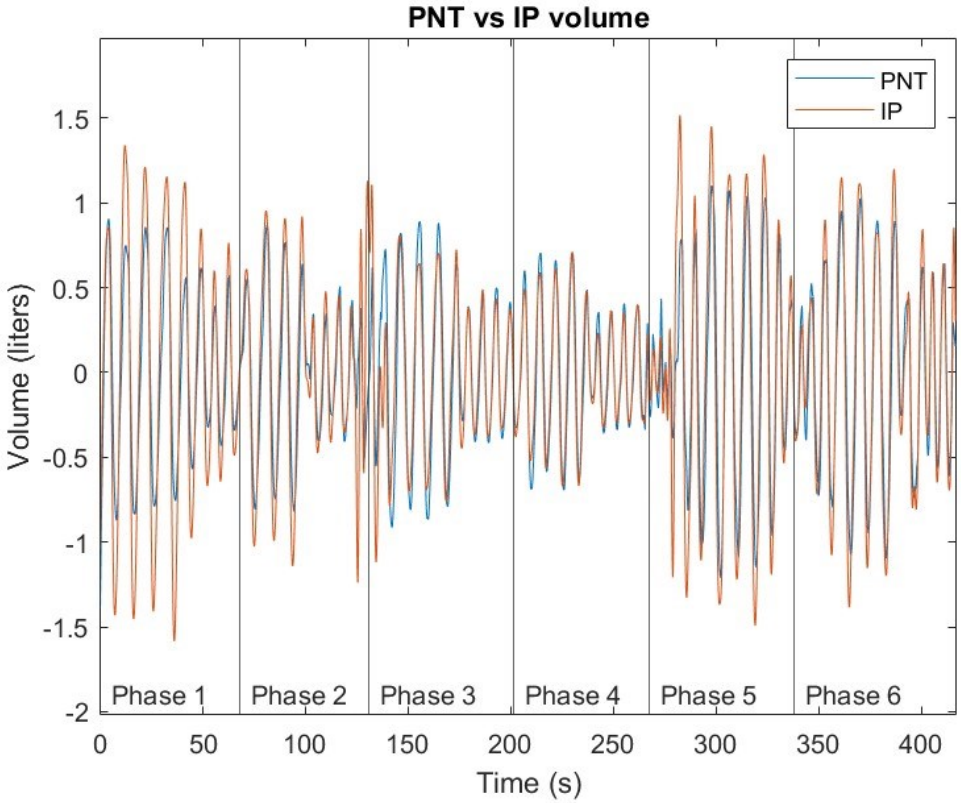

Figure 16. *Breath volume signal (blue) and corresponding amplitude scaled IP signal (red) of subject 5 with Mason-Likar arm electrodes*

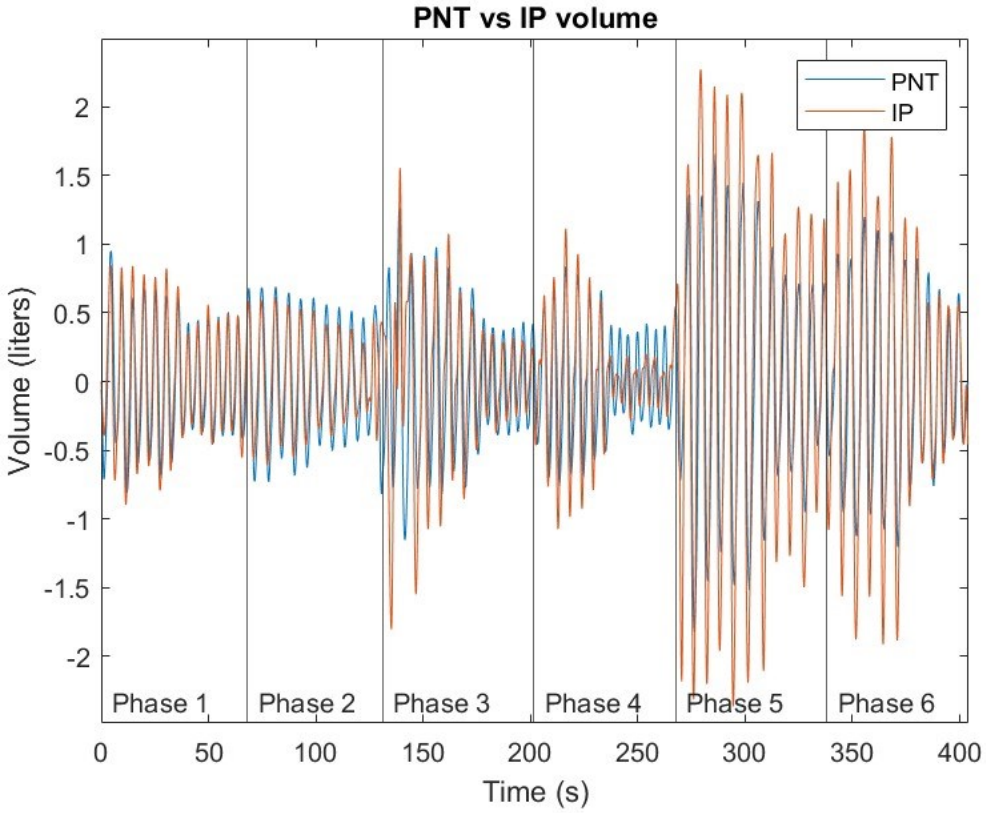

Figure 17. *Breath volume signal (blue) and corresponding amplitude scaled IP signal (red) of subject 1 with V5 electrodes*

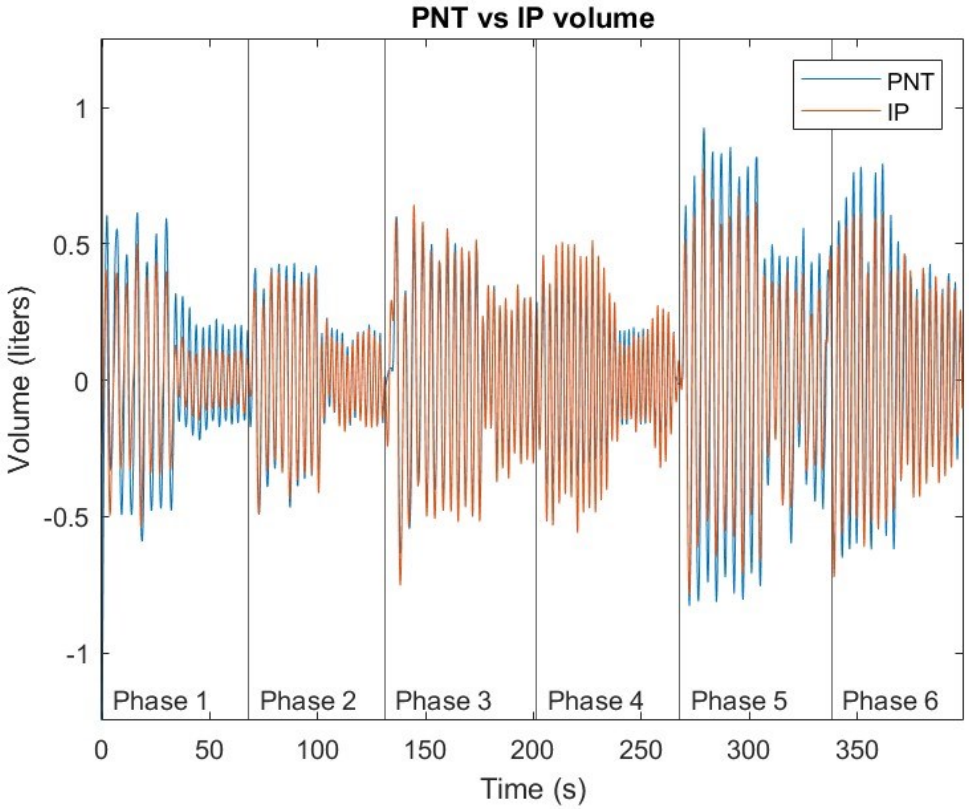

Figure 18. *Breath volume signal (blue) and corresponding amplitude scaled IP signal (red) of subject 2 with V5 electrodes*

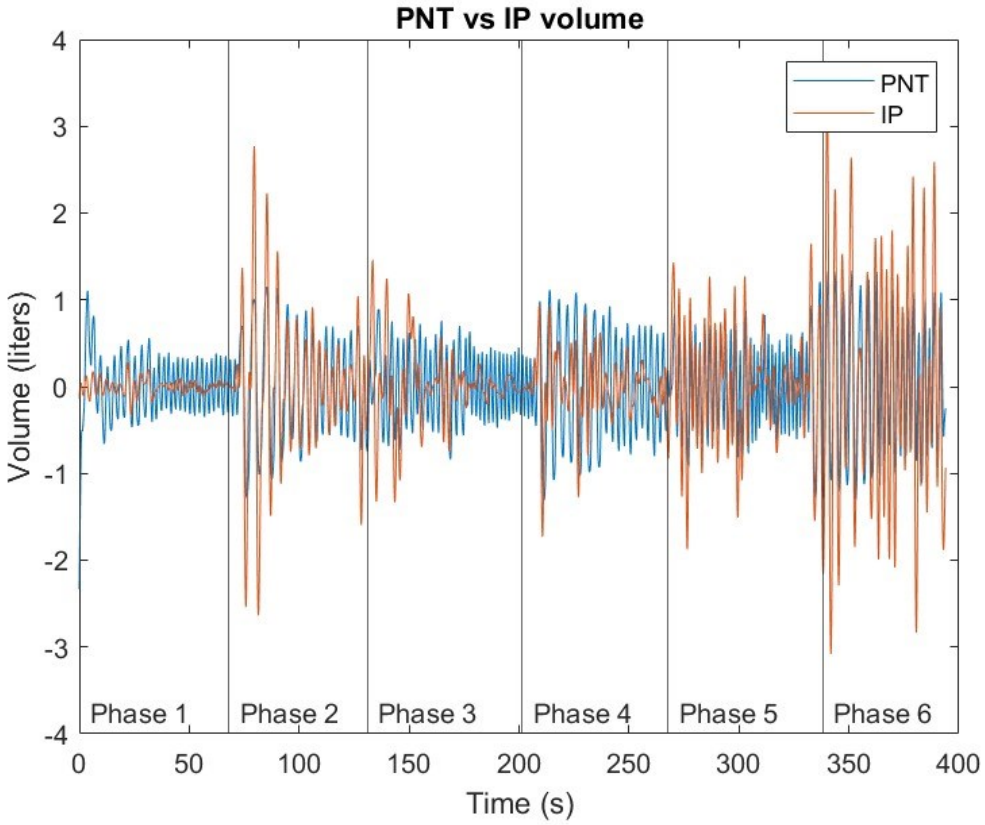

Figure 19. *Breath volume signal (blue) and corresponding amplitude scaled IP signal (red) of subject 3 with V5 electrodes*

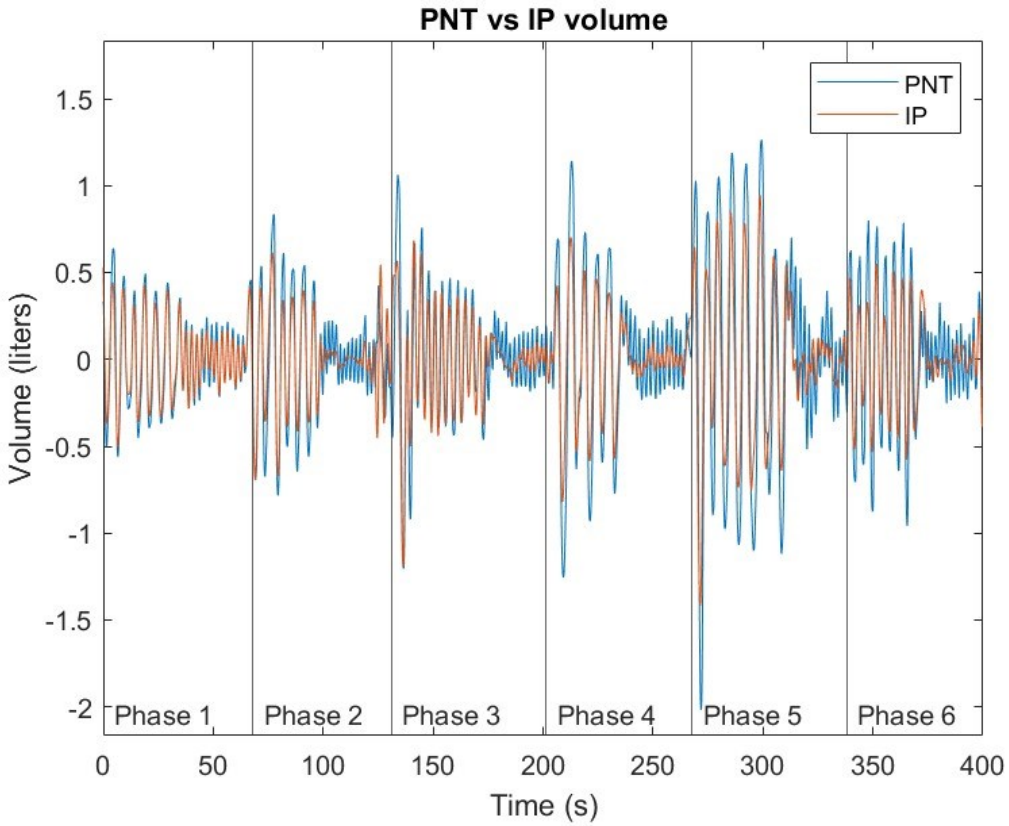

Figure 20. *Breath volume signal (blue) and corresponding amplitude scaled IP signal (red) of subject 4 with V5 electrodes*

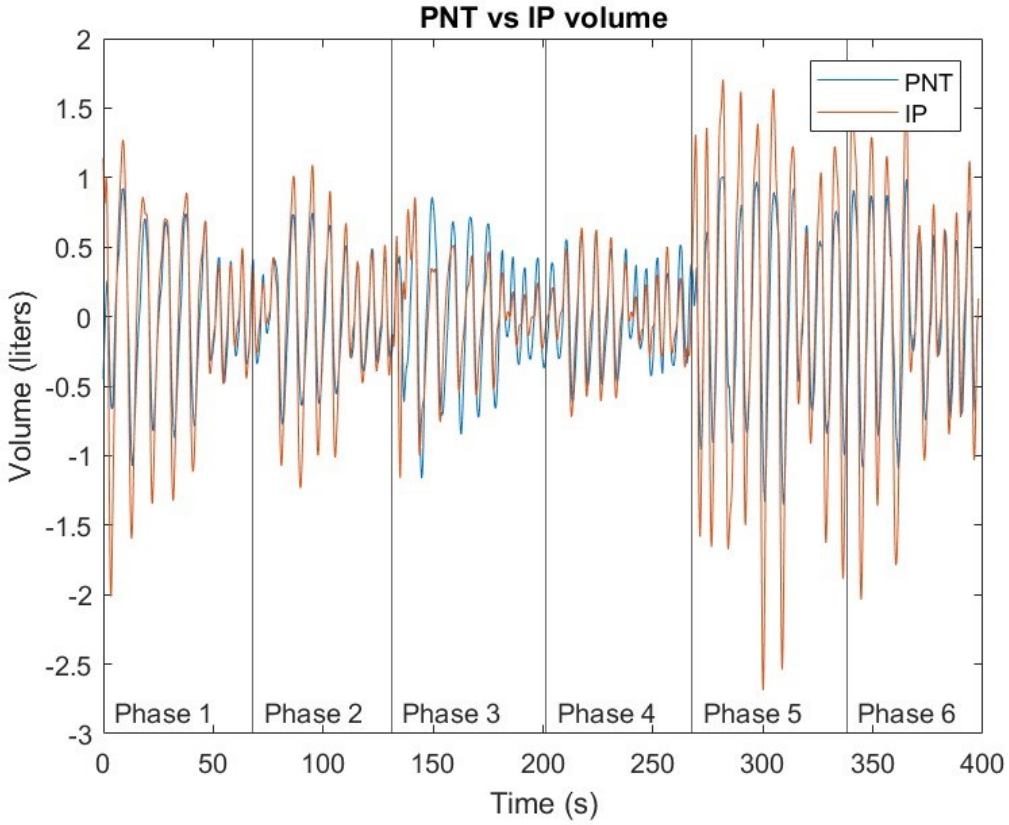

Figure 21. *Breath volume signal (blue) and corresponding amplitude scaled IP signal (red) of subject 5 with V5 electrodes*